# 横浜国立大学理科紀要

第一類 数学 物理学

第 三 輯

# SCIENCE REPORTS
## OF THE
# YOKOHAMA NATIONAL UNIVERSITY

SECTION I

MATHEMATICS, PHYSICS

No. 3

FACULTY OF LIBERAL ARTS AND EDUCATION
YOKOHAMA NATIONAL UNIVERSITY
KAMAKURA, JAPAN

MARCH, 1954

$$\xi^{\kappa}_{;\tau} V^{\tau}_{\kappa i} + \xi^{\kappa} V_{\kappa i} = 0 . \tag{3}$$

As it is well-known that if we have $R^{\lambda}_{\cdot\mu\nu\omega}=0$, the space admits a group of affine motions of maximum order $n^2+n$ and vice versa, we consider only the case $R^{\lambda}_{\cdot\mu\nu\omega} \neq 0$, $n \geqq 3$, and assume $r=n^2$, for we shall show later (§ 3) that if $R^{\lambda}_{\cdot\mu\nu\omega} \neq 0$, $r$ can not be more than $n^2$ [I. P. Egorov, 1]. As there are just $n$ equations in (3), $i$ can take on $1, \cdots\cdots, n$, and we may treat $i$ as a covariant index, for the equations in (3) may be substituted by linear combinations of them.

## § 2. Curvature affinor of an $A_n$ admitting a group of affine motions of order $n^2$.

As the equations (2) must be linear combinations of (3), we get

$$R^{\lambda}_{\cdot\mu\nu\omega;\sigma} = -A^{\alpha\lambda}_{\cdot\cdot\mu\nu\omega} V_{\sigma\alpha} , \tag{4}$$

$$R^{\tau}_{\cdot\mu\nu\omega}\delta^{\lambda}_{\kappa} - R^{\lambda}_{\cdot\kappa\nu\omega}\delta^{\tau}_{\mu} - R^{\lambda}_{\cdot\mu\kappa\omega}\delta^{\tau}_{\nu} - R^{\lambda}_{\cdot\mu\nu\kappa}\delta^{\tau}_{\omega} = A^{\alpha\lambda}_{\cdot\cdot\mu\nu\omega} V^{\tau}_{\kappa\alpha} . \tag{5}$$

We first treat (5) to find the form of $R^{\lambda}_{\cdot\mu\nu\omega}$.

The first thing to do is to eliminate $A^{\alpha\lambda}_{\cdot\cdot\mu\nu\omega}$, and we first consider the case where there is some vector $u^{\kappa}$ such that the determinant $|V^{\lambda}_{\kappa\mu}u^{\kappa}|$ does not vanish, for we can prove later (§ 3) that if this determinant vanishes for any vector $u^{\kappa}$, we have $R^{\lambda}_{\cdot\mu\nu\omega}=0$, and this contradicts the assumption $r=n^2$.

As $|V^{\lambda}_{\kappa\mu}u^{\kappa}| \neq 0$, we can find out an affinor $V^{\beta}_{\tau}$ such that $V^{\tau}_{\kappa\mu}u^{\kappa}V^{\beta}_{\tau}=\delta^{\beta}_{\mu}$. Then multiplying (5) by $u^{\kappa}V^{\beta}_{\tau}$ and contracting, we get

$$A^{\beta\lambda}_{\cdot\cdot\mu\nu\omega} = V^{\beta}_{\tau} R^{\tau}_{\cdot\mu\nu\omega} u^{\lambda} - R^{\lambda}_{\cdot\kappa\nu\omega} u^{\kappa} V^{\beta}_{\mu} - R^{\lambda}_{\cdot\mu\kappa\omega} u^{\kappa} V^{\beta}_{\nu} - R^{\lambda}_{\cdot\mu\nu\kappa} u^{\kappa} V^{\beta}_{\omega} ,$$

and substituting these into (5), we get equations of the form

$$R^{\tau}_{\cdot\mu\nu\omega}\delta^{\lambda}_{\kappa} - R^{\lambda}_{\cdot\kappa\nu\omega}\delta^{\tau}_{\mu} - R^{\lambda}_{\cdot\mu\kappa\omega}\delta^{\tau}_{\nu} - R^{\lambda}_{\cdot\mu\nu\omega}\delta^{\tau}_{\omega} = [\cdots\cdots] u^{\lambda} - R^{\lambda}_{\cdot\alpha\nu\omega} u^{\alpha} W^{\tau}_{\kappa\mu} - R^{\lambda}_{\cdot\mu\alpha\omega} u^{\alpha} W^{\tau}_{\kappa\nu} - R^{\lambda}_{\cdot\mu\nu\alpha} u^{\alpha} W^{\tau}_{\kappa\omega} , \tag{6}$$

where $W^{\tau}_{\kappa\mu} = V^{\beta}_{\mu} V^{\tau}_{\kappa\beta}$.

Then we take a covariant vector $a_{\sigma}$ and a contravariant vector $v^{\sigma}$ such that $u^{\sigma}a_{\sigma} = v^{\sigma}a_{\sigma} = 0$, and multiply (6) by $a_{\lambda}v^{\kappa}$. On contracting, we get

$$R^{\lambda}_{\cdot\kappa\nu\omega} a_{\lambda} v^{\kappa} \delta^{\tau}_{\mu} + R^{\lambda}_{\cdot\mu\kappa\omega} a_{\lambda} v^{\kappa} \delta^{\tau}_{\nu} + R^{\lambda}_{\cdot\mu\nu\kappa} a_{\lambda} v^{\kappa} \delta^{\tau}_{\omega} - R^{\lambda}_{\cdot\alpha\nu\omega} a_{\lambda} u^{\alpha} W^{\tau}_{\mu} - R^{\lambda}_{\cdot\mu\alpha\omega} a_{\lambda} u^{\alpha} W^{\tau}_{\nu} - R^{\lambda}_{\cdot\mu\nu\alpha} a_{\lambda} u^{\alpha} W^{\tau}_{\omega} = 0 \tag{7}$$

where $W^{\tau}_{\mu} = W^{\tau}_{\kappa\mu} u^{\kappa}$. These equations have the form

$$(8)\qquad L_{\nu\omega}\,\delta^\tau_\mu+M_{\mu\omega}\,\delta^\tau_\nu-M_{\mu\nu}\,\delta^\tau_\omega$$
$$-C_{\nu\omega}W^\tau_\mu-D_{\mu\omega}\,W^\tau_\nu+D_{\mu\nu}\,W^\tau_\omega=0$$

with $\quad L_{\nu\omega}=M_{\nu\omega}-M_{\omega\nu}\,,\qquad C_{\nu\omega}=D_{\nu\omega}-D_{\omega\nu}\,,$

if we put $\quad L_{\nu\omega}=R^\alpha_{\cdot\beta\nu\omega}\,a_\alpha v^\beta\,,\qquad M_{\mu\omega}=R^\alpha_{\cdot\mu\beta\omega}\,a_\alpha v^\beta\,,$

$$C_{\nu\omega}=R^\alpha_{\cdot\beta\nu\omega}\,a_\alpha u^\beta\,,\qquad D_{\mu\omega}=R^\alpha_{\cdot\mu\beta\omega}\,a_\alpha u^\beta\,,$$

for we have $R^\lambda_{\cdot[\mu\nu\omega]}=0$ and $R^\lambda_{\cdot\mu(\nu\omega)}=0$. Then owing to the lemma proved in the appendix of this paper, we can conclude

$$(9)\qquad M_{\mu\nu}=\alpha D_{\mu\nu}\,.$$

These equations mean

$$(10)\qquad R^\alpha_{\cdot\mu\beta\nu}\,a_\alpha v^\beta=\alpha R^\alpha_{\cdot\mu\beta\nu}\,a_\alpha u^\beta\,,$$

in which $\alpha$ is an unknown quantity and the vectors $u^\lambda$, $v^\lambda$, and $a_\lambda$ must satisfy $|V^\lambda_{\kappa\mu}u^\kappa|\neq 0$ and $u^\sigma a_\sigma=v^\sigma a_\sigma=0$. But as the former inequality is satisfied by an arbitrary vector $u^\lambda$ as long as it is sufficiently near some fixed vectors, only the latter equalities are to be taken into account. As we get from (10) $R^\alpha_{\cdot\mu\beta\gamma}\,a_\alpha v^\beta u^\gamma=0$, we have

$$(11)\qquad R^\lambda_{\cdot\mu\beta\gamma}\,v^\beta u^\gamma=u^\lambda A_\mu+v^\lambda B_\mu\,,$$

where $A_\mu$ and $B_\mu$ are unknown vectors, which will depend upon $u^\lambda$ and $v^\lambda$.

Now we can take $u^\lambda$ and $v^\lambda$ arbitrarily, for we can take the equations $u^\sigma a_\sigma=0$, $v^\sigma a_\sigma=0$ as the equations confining $a_\lambda$, but not $u^\lambda$ and $v^\lambda$. If we put $u^\lambda=\delta^\lambda_2$, $v^\lambda=\delta^\lambda_3$, we get from (11) $R^1_{\cdot\mu 23}=0$[2]. Similarly, we get $R^i_{\cdot\mu jk}=0$ for $i\neq j$, $i\neq k$, and this is true with almost any coordinate system[2]. If we change this, we get, for example, $R^\alpha_{\cdot\mu\beta\gamma}A^1_\alpha B^\beta_2 B^\gamma_3=0$, where $A^\lambda_\mu=\partial y^\lambda/\partial x^\mu$, $B^\lambda_\mu=\partial x^\lambda/\partial y^\mu$. Put $A^\lambda_\mu=\delta^\lambda_\mu+t\delta^\lambda_1\,\delta^2_\mu$, $B^\lambda_\mu=\delta^\lambda_\mu-t\delta^\lambda_1\,\delta^2_\mu$, at the point $(x^\lambda)_0$ in question, then we get $R^\alpha_{\cdot\mu\beta\gamma}(\delta^1_\alpha+t\delta^2_\alpha)\,(\delta^\beta_2-t\delta^\beta_1)\delta^\gamma_3=0$, that is, $R^2_{\cdot\mu 23}=R^1_{\cdot\mu 13}$. Similarly, we get

$$R^2_{\cdot\mu 21}=R^3_{\cdot\mu 31}=\ \cdots\cdots\ =R^n_{\cdot\mu n1}$$
$$R^1_{\cdot\mu 12}=R^3_{\cdot\mu 32}=\ \cdots\cdots\ =R^n_{\cdot\mu n2}$$
$$\cdots\cdots\qquad\qquad\cdots\cdots\,,$$

and from these facts we get at last

$$(12)\qquad R^\lambda_{\cdot\mu\nu\omega}=\delta^\lambda_\nu A_{\mu\omega}-\delta^\lambda_\omega A_{\mu\nu}\,.$$

As this affinor must satisfy $R^\lambda_{\cdot[\mu\nu\omega]}=0$, we have $A_{\mu\nu}=A_{\nu\mu}$.

Substituting (12) into (10), these become $A_{\mu\beta}\,v^\beta=\alpha A_{\mu\beta}\,u^\beta$. In these equations $u^\lambda$ and $v^\lambda$ are arbitrary, while $A_{\mu\nu}$ are independent of $u^\lambda$ and $v^\lambda$, for

(2) It may happen that $u^\lambda=\delta^\lambda_2$ make $|V^\lambda_{\kappa\mu}u^\kappa|=0$, but remark that we can take such a coordinate system that $|V^\lambda_{\kappa\mu}u^\kappa|\neq 0$ is fulfilled by any one of $u^\lambda=\delta^\lambda_1$, ....., $u^\lambda=\delta^\lambda_n$.

we have (12). Then we know that the affinor $A_{\mu\nu}$ has the form $A_{\mu\nu}=A_\mu B_\nu$, and as $A_{\mu\nu}$ is symmetric, we get $A_{\mu\nu}=RB_\mu B_\nu$. Hence $R^\lambda_{\cdot\mu\nu\omega}$ has the form

$$R^\lambda_{\cdot\mu\nu\omega}=RB_\mu(\delta^\lambda_\nu B_\omega-\delta^\lambda_\omega B_\nu). \tag{13}$$

We postpone further discussions a little and treat

## §3. The case where $|V^\lambda_{\kappa\mu}u^\kappa|=0$ for any $u^\kappa$.

In this case we can find out a vector $W_\tau$ for each vector $u^\kappa$, such that we have

$$V^\tau_{\kappa\mu}u^\kappa W_\tau=0. \tag{14}$$

Then multiplying (5) by $u^\kappa W_\tau$ and contracting, we get

$$R^\tau_{\cdot\mu\nu\omega}W_\tau u^\lambda=R^\lambda_{\cdot\kappa\nu\omega}u^\kappa W_\mu+R^\lambda_{\cdot\mu\kappa\omega}u^\kappa W_\nu+R^\lambda_{\cdot\mu\nu\kappa}u^\kappa W_\omega. \tag{15}$$

Multiplying these by an arbitrary vector $a^\mu$ and contracting, we get

$$R^\lambda_{\cdot\kappa\nu\omega}u^\kappa W_\alpha a^\alpha=u^\lambda R^\tau_{\gamma\omega}W_\tau+R^\lambda_{\kappa\nu}u^\kappa W_\omega-R^\lambda_{\kappa\omega}u^\kappa W_\nu, \tag{16}$$

where $R^\lambda_{\gamma\omega}=R^\lambda_{\cdot\mu\nu\omega}a^\mu$. Multiply (15) by $u^\mu$ and contract, substitute (16) into the resulting equations then we get

$$(u^\lambda R^\tau_{\alpha\omega}u^\alpha W_\tau-R^\lambda_{\alpha\omega}u^\alpha W_\beta u^\beta)W_\nu$$
$$=(u^\lambda R^\tau_{\alpha\nu}u^\alpha W_\tau-R^\lambda_{\alpha\nu}u^\alpha W_\beta u^\beta)W_\omega.$$

From these equations we obtain

$$u^\lambda R^\tau_{\alpha\nu}u^\alpha W_\tau-R^\lambda_{\alpha\nu}u^\alpha W_\beta u^\beta=\alpha^\lambda W_\nu. \tag{17}$$

Multiply these by $u^\nu$ and contract, then we get $\alpha^\lambda W_\nu u^\nu=0$ because of $R^\lambda_{(\mu\nu)}=0$. This means $\alpha^\lambda=0$ or $W_\nu u^\nu=0$, hence we get

$$R^\lambda_{\alpha\nu}u^\alpha=\frac{[\cdots]}{W_\alpha u^\alpha}u^\lambda \tag{18}$$

or

$$W_\nu u^\nu=0, \qquad W_\lambda R^\lambda_{\alpha\nu}u^\alpha=\alpha W_\nu. \tag{19}$$

If (18) is true, we have $R^\lambda_{\cdot\mu\nu\omega}a^\mu u^\nu=u^\lambda\pi_\omega$, where $\pi_\omega$ is an unknown vector. As $a^\mu$ is arbitrary, we get $R^\lambda_{\cdot\mu\nu\omega}u^\nu=u^\lambda\pi_{\mu\omega}$ with unknown $\pi_{\mu\omega}$. If we put $u^\lambda=\delta^\lambda_1$, we get $R^i_{\cdot\mu1\omega}=0$ for $i\neq1$. We can obtain a set of similar equations, and as $R^\lambda_{\cdot\mu(\nu\omega)}=0$, we can conclude $R^\lambda_{\cdot\mu\nu\omega}=0$. Hence this case must be discarded.

Let us consider the case where (19) holds.

Then multiplying (15) by $u^\nu$ and contracting, we get

$$R^\lambda_{\cdot\alpha\beta\omega}u^\alpha u^\beta=[\cdots\cdots]u^\lambda,$$

because of $W_\nu u^\nu=0$ and $R^\lambda_{\cdot\mu\nu\kappa}u^\nu u^\kappa=0$. As $u^\lambda$ are arbitrary, we get, as a

result of some calculation usual in tensor calculus, and such as used in obtaining (12),

$$R^{\lambda}_{\cdot\mu\nu\omega}+R^{\lambda}_{\cdot\nu\mu\omega}=B_{\omega\mu}\,\delta^{\lambda}_{\nu}+B_{\omega\nu}\,\delta^{\lambda}_{\mu}, \tag{20}$$

where $B_{\mu\nu}$ is an unknown affinor.

As we have $R^{\lambda}_{\cdot[\mu\nu\omega]}=0$, we get from (20)

$$2R^{\lambda}_{\cdot\nu\mu\omega}-R^{\lambda}_{\cdot\omega\mu\nu}=B_{\omega\mu}\,\delta^{\lambda}_{\nu}+B_{\omega\nu}\,\delta^{\lambda}_{\mu}.$$

Exchange $\nu$ and $\omega$ and multiply the resulting equations by 2 and add them to the former ones, then we get

$$3R^{\lambda}_{\cdot\omega\mu\nu}=(2B_{\nu\omega}+B_{\omega\nu})\delta^{\lambda}_{\mu}+2B_{\nu\mu}\,\delta^{\lambda}_{\omega}+B_{\omega\mu}\,\delta^{\lambda}_{\nu}.$$

But as $R^{\lambda}_{\cdot\mu(\nu\omega)}=0$, we get

$$(B_{\nu\omega}+B_{\omega\nu})\delta^{\lambda}_{\mu}+(B_{\nu\mu}+B_{\mu\nu})\delta^{\lambda}_{\omega}+(B_{\mu\omega}+B_{\omega\mu})\delta^{\lambda}_{\nu}=0,$$

from which we can conclude $B_{\mu\nu}+B_{\nu\mu}=0$. Hence we have

$$R^{\lambda}_{\cdot\mu\nu\omega}=\frac{1}{3}(B_{\mu\nu}\,\delta^{\lambda}_{\omega}-B_{\mu\omega}\,\delta^{\lambda}_{\nu}+2B_{\nu\omega}\,\delta^{\lambda}_{\mu}). \tag{21}$$

It seems that we can draw no more useful results from (5). Therefore we substitute (21) into the Bianchi's identity $R^{\lambda}_{\cdot\mu[\nu\omega;\sigma]}=0$, and get

$$6\,\delta^{\lambda}_{\mu}\,B_{[\nu\omega;\sigma]}+\delta^{\lambda}_{\nu}\,(B_{\mu\omega;\sigma}-B_{\mu\sigma;\omega})$$

$$+\delta^{\lambda}_{\omega}\,(B_{\mu\sigma;\nu}-B_{\mu\nu;\sigma})+\delta^{\lambda}_{\sigma}\,(B_{\mu\nu;\omega}-B_{\mu\omega;\nu})=0.$$

Contracting with respect to $\lambda$ and $\sigma$ and taking into account of $B_{\mu\nu}+B_{\nu\mu}=0$, we get

$$2\,B_{\nu\omega;\mu}+n\,(B_{\mu\nu;\omega}-B_{\mu\omega;\nu})=0, \tag{22}$$

and taking the symmetric part with respect to $\mu$ and $\nu$, we get $B_{\mu\omega;\nu}+B_{\nu\omega;\mu}=0$ for $n\geqq 3$. Hence $B_{\mu\nu;\omega}$ is skew-symmetric in all indices and we obtain

$$B_{\mu\nu;\omega}=0$$

from (22).

Differentiating covariantly, we get $B_{\mu\nu;\omega;\sigma}=0$, hence $R^{\varpi}_{\cdot\mu\omega\sigma}\,B_{\varpi\nu}+R^{\varpi}_{\cdot\nu\omega\sigma}\,B_{\mu\varpi}=0$. Substituting (21) into these equations, we get, after some calculation, $2B_{\mu\nu}\,B_{\omega\sigma}+B_{\omega\nu}\,B_{\mu\sigma}-B_{\sigma\nu}\,B_{\mu\omega}=0$. Taking the symmetric part of these equations with respect to $\nu$ and $\sigma$, we get $B_{\mu\nu}\,B_{\omega\sigma}+B_{\mu\sigma}\,B_{\omega\nu}=0$, hence $B_{\mu\nu}$ must have the form $B_{\mu\nu}=A_{\mu}\,B_{\nu}$ with unknown $A_{\mu}$ and $B_{\nu}$. But we know $B_{\mu\nu}=-B_{\nu\mu}$, and consequently we obtain $B_{\mu\nu}=0$ and $R^{\lambda}_{\cdot\mu\nu\omega}=0$. Then we get the

Lemma: *An affinely connected space $A_n$ with non-vanishing curvature affinor can not have the curvature affinor satisfying* (21) *for* $n\geqq 3$.

Thus we must discard the case $|V^{\lambda}_{\kappa\mu}\,u^{\kappa}|=0$.

But here we have an interesting remark.

Suppose that we have a group of affine motions with maximum order

$r$, $n^2 < r < n^2+n$. Then we have equations (3) with $i=1,\cdots, n^2+n-r$, but we can fill the vacant ones, $i=n^2+n-r+1,\cdots n$, formally by $0\times\xi^\kappa_{;\tau}+0\times\xi^\kappa=0$. The determinant $|V^\lambda_{\kappa\mu}u^\kappa|$ thus obtained is always null and we get the

Theorem: *An affinely connected space can not have a complete group of affine motions of order* $r$, $n^2 < r < n^2+n$ [Egorov, 1].

## § 4. Relations obtained from $XR^\lambda_{\cdot\mu\nu\omega}=0$ and $X(R^\lambda_{\cdot\mu\nu\omega;\sigma})=0$.

We return to the equations (13) and rewrite them as

$$R^\lambda_{\cdot\mu\nu\omega}=eA_\mu(\delta^\lambda_\nu A_\omega-\delta^\lambda_\omega A_\nu), \tag{23}$$

where $e=\pm1$. Substituting these into $XR^\lambda_{\cdot\mu\nu\omega}=0$, we get

$$[(XA_\mu)A_\omega+A_\mu XA_\omega]\delta^\lambda_\nu-[(XA_\mu)A_\nu+A_\mu XA_\nu]\delta^\lambda_\omega=0,$$

hence

$$(XA_\mu)A_\nu+A_\mu XA_\nu=0, \tag{24}$$

from which we soon obtain $XA_\mu=\varphi A_\mu$, and substituting these into (24) we find

$$XA_\mu=0, \tag{25}$$

that is, $A_{\mu;\sigma}\xi^\sigma+A_\sigma\xi^\sigma_{;\mu}=0$ or

$$\xi^\kappa_{;\tau}\delta^\tau_\mu A_\kappa+\xi^\kappa A_{\mu;\kappa}=0. \tag{26}$$

As there are *just* $n$ linearly independent equations in (26), we know that (26) is equivalent to (3).

Substituting (23) into $X(R^\lambda_{\cdot\mu\nu\omega;\sigma})=0$, we get

$$X[A_{\mu;\sigma}(\delta^\lambda_\nu A_\omega-\delta^\lambda_\omega A_\nu)+A_\mu(\delta^\lambda_\nu A_{\omega;\sigma}-\delta^\lambda_\omega A_{\nu;\sigma})]=0,$$

from which we obtain

$$X(A_{\mu;\sigma})A_\omega+A_\mu X(A_{\omega;\sigma})=0,$$

hence

$$X(A_{\mu;\nu})=0,$$

which mean $A_{\mu;\nu;\sigma}\xi^\sigma+A_{\sigma;\nu}\xi^\sigma_{;\mu}+A_{\mu;\sigma}\xi^\sigma_{;\nu}=0$ or

$$\xi^\kappa_{;\tau}[A_{\kappa;\nu}\delta^\tau_\mu+A_{\mu;\kappa}\delta^\tau_\nu]+\xi^\kappa A_{\mu;\nu;\kappa}=0. \tag{27}$$

But these equations must be satisfied whenever our condition (3) or (26) is satisfied, hence we have

$$A_{\kappa;\nu}\delta^\tau_\mu+A_{\mu;\kappa}\delta^\tau_\nu=L^{\cdot\cdot\alpha}_{\mu\nu}\delta^\tau_\alpha A_\kappa=L^{\cdot\cdot\tau}_{\mu\nu}A_\kappa, \tag{28}$$

$$A_{\mu;\nu;\kappa}=L^{\cdot\cdot\alpha}_{\mu\nu}A_{\alpha;\kappa}, \tag{29}$$

which mean that the equations in (27) are linear combinations of the equations in (26).

Contracting with respect to $\tau$ and $\mu$, we get from (28)

$$nA_{\kappa;\nu}+A_{\nu;\kappa}=L^{\cdot\cdot\alpha}_{\alpha\nu}A_\kappa . \tag{30}$$

Similarly, we get $A_{\kappa;\mu}+nA_{\mu;\kappa}=L^{\cdot\cdot\alpha}_{\mu\alpha}A_\kappa$, hence

$$A_{\kappa;\nu}+nA_{\nu;\kappa}=L^{\cdot\cdot\alpha}_{\nu\alpha}A_\kappa . \tag{31}$$

From (30) and (31) we get

$$(n^2-1)A_{\kappa;\nu}=(nL^{\cdot\cdot\alpha}_{\alpha\nu}-L^{\cdot\cdot\alpha}_{\nu\alpha})A_\kappa$$

and

$$(n^2-1)A_{\nu;\kappa}=(nL^{\cdot\cdot\alpha}_{\nu\alpha}-L^{\cdot\cdot\alpha}_{\alpha\nu})A_\kappa ,$$

and from these equations we can deduce

$$A_{\mu;\nu}=aA_\mu A_\nu . \tag{32}$$

Substituting (32) into (28), we get

$$L^{\cdot\cdot\lambda}_{\mu\nu}=a(A_\nu\delta^\lambda_\mu+A_\mu\delta^\lambda_\nu) , \tag{33}$$

and substituting these equations and (32) into the right hand side of (29), we get

$$A_{\mu;\nu;\kappa}=2a^2A_\mu A_\nu A_\kappa .$$

On the other hand, we have $A_{\mu;\nu;\kappa}=2a^2A_\mu A_\nu A_\kappa+a_{;\kappa}A_\mu A_\nu$ from (32). Therefore we get $a_{;\kappa}=0$ and

$$a=\text{constant}. \tag{34}$$

## § 5. The expression of an $A_n$ admitting a group of affine motions of order $n^2$ in tensor form.

All that we obtained hitherto is the set of relations

$$\begin{cases} R^\lambda_{\cdot\mu\nu\omega}=eA_\mu(\delta^\lambda_\nu A_\omega-\delta^\lambda_\omega A_\nu) \\ A_{\mu;\nu}=aA_\mu A_\nu , \\ a=\text{constant}, \qquad A_\mu\neq 0 , \end{cases} \tag{35}$$

as the necessary condition for an $A_n$ to have a group of affine motions of order $n^2$. The equations for the vector $\xi^\lambda$ are

$$\xi^\kappa_{;\mu}A_\kappa+aA_\mu\xi^\kappa A_\kappa=0 . \tag{36}$$

That (35) is the necessary and sufficient condition is found at once. Because of (35) we have

$$R^\lambda_{\cdot\mu\nu\omega;\sigma_1;\cdots;\sigma_m}=(m+1)!\,a^m eA_\mu(\delta^\lambda_\nu A_\omega-\delta^\lambda_\omega A_\nu)A_{\sigma_1}\cdots A_{\sigma_m} ,$$

and as we have $XA_\mu=0$ already, we soon find

$$X(R^\lambda_{\cdot\mu\nu\omega;\sigma_1;\cdots;\sigma_m})=0 .$$

The last thing to do is to prove the existence of an $A_n$ satisfying (35), but this problem was already solved by Egorov by finding an example

[Egorov, 1]. I do not represent it here, but instead, in the next section, I solve (35) using a suitable coordinate system. As a result we have the

Theorem: *An affinely connected space $A_n$ with non-vanishing curvature affinor has no group of affine motions of order more than $n^2$. It has a complete group of affine motions of order $n^2$ if and only if the condition* (35) *is satisfied, and such spaces really exist.*

## § 6. The property of an $A_n$ fulfilling (35) and the complete group of affine motions in this $A_n$.

We find that $A_\mu$ is a gradient vector, $A_\mu=f_{,\mu}$, for $A_{\mu,\nu}-A_{\nu,\mu}=0$. Then we can take a coordinate system such that $f=x^n$, and get

$$A_\mu=\delta^n_\mu. \tag{37}$$

Because of (32) we soon find

$$\Gamma^n_{j\nu}=\Gamma^n_{\mu k}=0, \tag{38}$$

for $i, j, k, \cdots=1, \cdots, n-1$.

From the expression of $R^\lambda_{\cdot\mu\nu\omega}$ we get, for $\lambda=i$,

$$\Gamma^i_{jk,h}-\Gamma^i_{jh,k}-\Gamma^a_{jh}\Gamma^i_{ak}+\Gamma^a_{jk}\Gamma^i_{ah}=0, \tag{39}$$

$$\Gamma^i_{jk,n}-\Gamma^i_{jn,k}-\Gamma^a_{jn}\Gamma^i_{ak}+\Gamma^a_{jk}\Gamma^i_{an}=0, \tag{40}$$

$$\Gamma^i_{nk,h}-\Gamma^i_{nh,k}-\Gamma^a_{nh}\Gamma^i_{ak}+\Gamma^a_{nk}\Gamma^i_{ah}=0, \tag{41}$$

$$\Gamma^i_{nk,n}-\Gamma^i_{nn,k}-\Gamma^a_{nn}\Gamma^i_{ak}-\Gamma^n_{nn}\Gamma^i_{nk}+\Gamma^a_{nk}\Gamma^i_{an}=e\delta^i_k. \tag{42}$$

Take a hypersurface $x^n=c$ and name it H($c$). In each H($c$) we can find out a set of $n-1$ independent parallel vector fields because of (39), and this means that we can find out a coordinate system such that

$$\Gamma^i_{jk}=0, \tag{43}$$

throughout the $A_n$. Besides, as we can choose the origin, $x^i=0$, in each H($c$) such that the locus of this point for variable $c$ forms a geodesic in the $A_n$, we can put

$$\Gamma^i_{nn}=0 \quad \text{for} \quad x^a=0, \tag{44}$$

because of $\ddot{x}^i+\Gamma^i_{\mu\nu}\dot{x}^\mu\dot{x}^\nu=\alpha\dot{x}^i$.

In taking a coordinate system, we have another freedom, the direction of the $(n-1)$-ple in H($c$), formed by the vectors $u^i_1=\delta^i_1, \cdots, u^i_{n-1}=\delta^i_{n-1}$ at the origin $x^i=0$. We can put them parallel along the geodesic $x^i=0$. Then we get

$$\Gamma^i_{kn}=0 \quad \text{for} \quad x^a=0, \tag{45}$$

because of $u^i_{k,n}+\Gamma^i_{an}u^a_k=0$ and $u^\lambda_k=\delta^\lambda_k$.

Substituting (43) into (40) and taking into account of (45), we get

(46) $$\Gamma^i_{jn}=0, \qquad \Gamma^i_{nk}=0$$

throughout the $A_n$. Similarly we get from (42) and (44)

(47) $$\Gamma^i_{nn}=-ex^i.$$

We get nothing more from (41).

The last parameter $\Gamma^n_{nn}$ is calculated from (32) when we put $\mu=\nu=n$, $\Gamma^n_{nn}=-a$.

All that we found is that the parameters $\Gamma^\lambda_{\mu\nu}$ are given by

(48) $$\Gamma^i_{nn}=-ex^i, \qquad \Gamma^n_{nn}=-a \quad \text{other } \Gamma^\lambda_{\mu\nu}=0.$$

We get no more relation from (35), and (48) is the complete solution of (35).

Now we are ready to find out the complete group of affine motions in the $A_n$ fulfilling (35).

From (36) we get $\xi^n_{;\mu}+a\xi^n\delta^n_\mu=0$, which becomes, because of (48), $\xi^n{}_{,j}=0$, $\xi^n{}_{,n}=0$, hence

(49) $$\xi^n=\text{constant},$$

while from (1) we get

(50) $$\xi^\lambda{}_{,\mu,\nu}+\xi^\alpha\Gamma^\lambda_{\mu\nu,\alpha}-\Gamma^\alpha_{\mu\nu}\xi^\lambda{}_{,\alpha}+\Gamma^\lambda_{\alpha\nu}\xi^\alpha{}_{,\mu}+\Gamma^\lambda_{\mu\alpha}\xi^\alpha{}_{,\nu}=0.$$

If we put $\lambda=i$ in (50), we get

$$\xi^i{}_{,j,k}=0$$

$$\xi^i{}_{,n,k}=0$$

$$\xi^i{}_{,n,n}+\Gamma^i_{nn,\alpha}\xi^\alpha-\Gamma^\alpha_{nn}\xi^i{}_{,\alpha}=0,$$

hence

$$\xi^i{}_{,j}=K^i_j, \qquad \xi^i=K^i_j x^i+fi(x^n),$$

$$fi''+afi'-efi=0.$$

If we put $\lambda=n$ in (50), we get no more relation. Hence we get

(51) $$\begin{cases} \xi^i=K^i_j x^j+A^i\exp(\alpha_1 x^n)+B^i\exp(\alpha_2 x^n) \\ \xi^n=K, \end{cases}$$

or

(52) $$\begin{cases} \xi^i=K^i_j x^j+(A^i+B^i x^n)\exp(\alpha x^n) \\ \xi^n=K, \end{cases}$$

where $K^i_j$, $A^i$, $B^i$, and $K$ are $n^2$ arbitrary constants, and $\alpha$'s satisfy $\alpha_1{}^2+a\alpha_1-e=0$, $\alpha_2{}^2+a\alpha_2-e=0$, $\alpha_1\neq\alpha_2$; $\alpha^2+\alpha a-e=0$, $2\alpha+a=0$.

A finite transformation of the group is easily found to be

(53) $$\begin{cases} x'^i=A^i_j x^j+A^i\exp(\alpha_1 x^n)+B^i\exp(\alpha_2 x^n) \\ x'^n=x^n+A, \end{cases}$$

or

$$(54)\qquad \begin{cases} x'^i = A^i_j\, x^j + (A^i + B^i\, x^n)\exp(\alpha x^n) \\ x'^n = x^n + A\,, \end{cases}$$

with $|A^i_j| > 0$.

We can resume the results in the

Theorem: *An affinely connected space $A_n$ with non-vanishing curvature affinor admits a complete group of affine motions of maximum order if and only if the equations*

$$R^\lambda_{\cdot\mu\nu\omega} = eA_\mu(\delta^\lambda_\nu A_\omega - \delta^\lambda_\omega A_\nu)\,,\quad A_{\mu;\nu} = aA_\mu A_\nu\,,\quad a=\text{constant}$$

*are satisfied. Then the order is $n^2$, and we can find out a coordinate system such that the coefficients of connection satisfy*

$$\Gamma^i_{nn} = -ex^i\,,\quad \Gamma^n_{nn} = -a\,,\qquad \text{other } \Gamma^\lambda_{\mu\nu} = 0\,,$$

*and a finite expression of the group is given by* (53) *or* (54) *according as the roots $\alpha_1$ and $\alpha_2$ of the equation $x^2+ax-e=0$ satisfy $\alpha_1 \neq \alpha_2$ or $\alpha_1=\alpha_2=\alpha$.*

## APPENDIX

We prove the

Lemma: *If we have the tensor equations*

$$(A1)\qquad L_{\nu\omega}\delta^\lambda_\mu + M_{\mu\omega}\delta^\lambda_\nu - M_{\mu\nu}\delta^\lambda_\omega - C_{\nu\omega}W^\lambda_\mu - D_{\mu\omega}W^\lambda_\nu + D_{\mu\nu}W^\lambda_\omega = 0$$

*and*

$$(A2)\qquad L_{\nu\omega} = M_{\nu\omega} - M_{\omega\nu}\,,\qquad C_{\nu\omega} = D_{\nu\omega} - D_{\omega\nu}$$

*for $n \geqq 3$, then we can conclude*

$$(A3)\qquad L_{\mu\nu} = M_{\mu\nu} = C_{\mu\nu} = D_{\mu\nu} = 0$$

*or*

$$(A4)\qquad M_{\mu\nu} = \alpha D_{\mu\nu}\,,$$

*where $\alpha$ is a scalar.*

Let us begin with the case $n \geqq 4$, for in this case we can prove the lemma easier.

First we assume $D_{\mu\nu}=0$. Then we have $C_{\mu\nu}=0$ and (A1) becomes $L_{\nu\omega}\delta^\lambda_\mu + M_{\mu\omega}\delta^\lambda_\nu - M_{\mu\nu}\delta^\lambda_\omega = 0$, from which we can find that (A3) is true.

We next assume $D_{\mu\nu}+D_{\nu\mu}=0$. Then we have

$$L_{\nu\omega}\delta^\lambda_\mu + M_{\mu\omega}\delta^\lambda_\nu - M_{\mu\nu}\delta^\lambda_\omega - 2D_{\nu\omega}W^\lambda_\mu - D_{\nu\omega}W^\lambda_\nu + D_{\mu\nu}W^\lambda_\omega = 0\,.$$

If we have some vector $W^\mu$ satisfying $M_{\mu\nu}W^\mu W^\nu \neq 0$, then we get

$$M_{\mu\nu}W^\mu W^\nu \delta^\lambda_\omega = W^\lambda(L_{\nu\omega} + M_{\nu\omega})W^\nu - 3(W^\lambda_\mu W^\mu)(D_{\nu\omega}W^\nu)\,,$$

hence $\delta^\lambda_\omega = W^\lambda T_\omega + U^\lambda V_\omega$ with some vectors $T_\omega$, $U^\lambda$, and $V_\omega$, which is not true for $n \geqq 3$. Therefore we know that $M_{\mu\nu} + M_{\nu\mu} = 0$, and (A1) becomes

$$2M_{\nu\omega}\,\delta^\lambda_\mu + M_{\mu\omega}\,\delta^\lambda_\nu - M_{\mu\nu}\,\delta^\lambda_\omega - 2D_{\nu\omega}\,W^\lambda_\mu - D_{\mu\omega}\,W^\lambda_\nu + D_{\mu\nu}\,W^\lambda_\omega = 0\,.$$

Taking the symmetric part with respect to $\mu$ and $\nu$, we get

$$M_{\mu\omega}\,\delta^\lambda_\nu + M_{\nu\omega}\,\delta^\lambda_\mu - D_{\mu\omega}\,W^\lambda_\nu - D_{\nu\omega}\,W^\lambda_\mu = 0\,,$$

and multiplying these equations by some vectors $c^\nu$ and $d^\omega$ and contracting, we find that the affinor $W^\lambda_\mu$ has the form

(A5) $$W^\lambda_\mu = \alpha\delta^\lambda_\mu + S^\lambda T_\mu + U^\lambda V_\mu\,.$$

If we assume $D_{\mu\nu} + D_{\nu\mu} \neq 0$, we can find out some vector $W^\lambda$ such as $D_{\mu\nu}\,W^\mu W^\nu \neq 0$. Multiplying (A1) by $W^\mu W^\nu$ and contracting, we get (A5) again with some $S^\lambda$, $T_\mu$, $U^\lambda$, and $V_\mu$.

Substituting (A5) into (A1) and putting $l_{\nu\omega} = L_{\nu\omega} - \alpha C_{\nu\omega}$, $m_{\mu\nu} = M_{\mu\nu} - \alpha D_{\mu\nu}$, we get

(A6) $$l_{\nu\omega}\,\delta^\lambda_\mu + m_{\mu\omega}\,\delta^\lambda_\nu - m_{\mu\nu}\,\delta^\lambda_\omega + [\cdots]\,S^\lambda + [\cdots]\,U^\lambda = 0\,.$$

If we multiply (A6) by a vector $a_\lambda$ satisfying $S^\lambda a_\lambda = U^\lambda a_\lambda = 0$, we get

(A7) $$l_{\nu\omega}\,a_\mu + m_{\mu\omega}\,a_\nu - m_{\mu\nu}\,a_\omega = 0\,.$$

Take such a coordinate system that at the point $(x^\lambda)_0$ in question we have $a_\lambda = \delta^1_\lambda$. Then if we put $\omega = 1$, $\mu \neq 1$, $\nu \neq 1$, we get $m_{jk} = 0$ for $j \neq 1$, $k \neq 1$, while if we put $\omega = 1$, $\mu = 1$, $\nu \neq 1$, we get $l_{j1} - m_{1j} = 0$, hence $m_{j1} = 2m_{1j}$ for $j \neq 1$. As $n \geqq 4$ we can find out another vector $b_\lambda$ satisfying $S^\lambda b_\lambda = U^\lambda b_\lambda = 0$, and let the coordinate system be such that $a_\lambda = \delta^1_\lambda$, $b_\lambda = \delta^2_\lambda$, at $(x^\lambda)_0$. Then we can deduce $m_{\mu\nu} = 0$, which mean (A4).

If $n = 3$ we can not find the vector $b_\lambda$ mentioned above. But according to a well-known property of matrices we can choose such a coordinate system that the components of the affinor $W^\lambda_\mu$ satisfy one of the following sets of equations;

(I) $$W^1_\mu = \alpha\delta^1_\mu\,, \quad W^2_\mu = \alpha'\delta^2_\mu\,, \quad W^3_\mu = \alpha''\delta^3_\mu\,,$$
$$\alpha \neq \alpha' \neq \alpha''\,,$$

(II) $$W^1_\mu = \alpha\delta^1_\mu\,, \quad W^2_\mu = \alpha\delta^2_\mu\,,$$

(III) $$W^1_\mu = \alpha\delta^1_\mu\,, \quad W^2_\mu = \alpha'\delta^2_\mu\,, \quad W^3_\mu = \delta^2_\mu + \alpha'\delta^3_\mu\,,$$
$$\alpha \neq \alpha'\,,$$

(IV) $$W^1_\mu = \alpha\delta^1_\mu\,, \quad W^2_\mu = \delta^1_\mu + \alpha\delta^2_\mu\,, \quad W^3_\mu = \delta^2_\mu + \alpha\delta^3_\mu\,,$$

at $(x^\lambda)_0$.

Let $\lambda$, $\mu$, $\nu$, and $\omega$ take on various values out of 1, 2, 3. We obtain some

sets of linear equations with $M_{\mu\nu}$ and $D_{\mu\nu}$ as unknowns, and it is a matter of simple exercises to solve them. We find

(I), (III) $D_{\mu\nu}=M_{\mu\nu}=0$,

(II), (IV) $M_{\mu\nu}=\alpha D_{\mu\nu}$,

hence (A3) or (A4) is true.

In concluding the paper, the author wishes to express his hearty thanks to Professor K. Yano, whose kind encouragement and valuable suggestions have made the completion of the present paper possible.

## References

Egorov, I. P., 1: Doklady Acad. Nauk (N. S.) SSSR, 57 (1947), 867-870.
Egorov, I. P., 2: ibd., 84 (1952), 209-212.
Mutō, Y.: Proc. Japan Acad., 26 (1950), 107-110.
Yano, K.: "*Groups of transformations in generalized spaces*", Academeia Press (1949).

I could not read the first two papers, which form a part of Egorov's excellent dissertations. According to the Math. Rev., Vol. 14, he obtained among other conditions (b) $R_{\alpha\beta}=(1-n)\,e\lambda_\alpha\lambda_\beta$, (c) $\lambda_{(\alpha;\beta)}=C\lambda_\alpha\lambda_\beta$, where $\lambda_{\alpha;\beta}$ satisfy $\lambda_{\alpha;[\beta}\lambda_{\gamma]}=0$. But then we have $\lambda_{\alpha;\beta}\lambda_\gamma=\lambda_{\alpha;\gamma}\lambda_\beta$, hence $\lambda_{\alpha;\beta}=\mu_\alpha\lambda_\beta$ with some vector $\mu_\alpha$. (c) becomes $\mu_\alpha\lambda_\beta+\mu_\beta\lambda_\alpha=2C\lambda_\alpha\lambda_\beta$, from which we get $\mu_\alpha=C\lambda_\alpha$, hence $\lambda_{\alpha;\beta}=C\lambda_\alpha\lambda_\beta$. Perhaps these equations correspond to my (32).

Added im proof: According to the Math. Rev., Vol. 14, No. 11, G. Vranceanu studied the same problem, but I could not read the original paper.

[Science Reports of the Yokohama National University, Sec. I, No. 3, 1954]

# Preliminary Report on the Magneto-thermoelectric Power of Nickel

By

**Nahonori MIYATA and Zenya FUNATOGAWA**

**Synopsis**

The magneto-thermoelectric powers of nickel are measured by the same method as in the case of iron. The results show positive signs and that (1) the magneto-thermoelectric power has a maximum at about -90°C and then decreases with decreasing temperatures and may tend to zero at 0°K, and (2) the magneto-thermoelectric powers between -90°C and about 300°C decrease with increasing temperatures but (3) in the neighbourhood of the Curie point they are negative signs and are produced by the additive magnetizations, which are proportional to the external magnetic fields, expected from the Weiss' theory.

## §1. Introduction

There are many investigations concerning the changes of thermo-electric forces of ferromagnetic substances such as iron and nickel, produced by magnetizations since the phenomena were discovered by W. Thomson. Recently one of the authors investigated the changes of thermoelectric powers of iron single crystals due to magnetizations and obtained many interesting results. We are now investigating the phenomena in the case of nickel by using the same apparatus and method described in the previous papers.[1]

The magneto-thermoelectric force is the thermal e.m.f. of the thermocouple consisting of a demagnetized specimen and the magnetized one, and is a difference between the two electromotive forces, each of which is measured against copper respectively, first for the demagnetized state of a specimen and then for the magnetized state of the same specimen subjected to external magnetic fields under the same temperature gradient in the specimen. In many previous papers the effects have been measured under the condition of the wide temperature differences between the cold and hot junctions, i.e., 100°C or more because the electromotive force of this couple is very small. It is unreasonable to discuss such results from theoretical view points because the magnetizations and thermoelectric powers may not change always with temperatures in a linear relation, so that we must define and measure the thermal e.m.f. as mean values between the temperatures $T+\frac{\Delta T}{2}$ and $T-\frac{\Delta T}{2}$

as in the case of ordinary thermoelectric powers. For simplicity, such defined e.m.f. is called the "magneto-thermoelectric power" or the "magneto-thermoelectric force per degree" at the given temperature $T$.

It is the purpose of this experiment to know the temperature dependency of the magneto-thermoelectric power of nickel and to compare it with the results of iron and also to give some fundamental knowledge to clear the mechanism of the interaction between the 3d- and 4s-electrons.

## § 2. Samples and results of measurements

The specimens of nickel are cylindrical rods, their diameters 1.00 mm. and lengths 25.3 cm.

The magneto-thermoelectric power is defined by $\left(\frac{\Delta E}{\Delta T}\right)_{mag}$ at $T$, as mentioned above, where $\Delta E$ noted by a galvanometer deflection is the induced thermoelectric force by the magnetization of the specimen when the temperatures of each end of the specimen keeps $T+\frac{\Delta T}{2}$ and $T-\frac{\Delta T}{2}$ respectively, under the condition that the ordinary thermal e.m.f. of the couple consisting of the specimen and lead wires is conpensated by a potentiometric connection. We have measured the temperature range between the boiling point of liquid oxygen and one above the Curie point under the condition that the $\Delta T$ is about 5°C~35°C and the maximum longitudinal external magnetic field is about 700 Oerstead.

A typical example of the results is shown in Fig. 1: the Fig. 1a is the magneto-thermoelectric power, which is positive sign, i.e., current flows from magnetized metal to de-

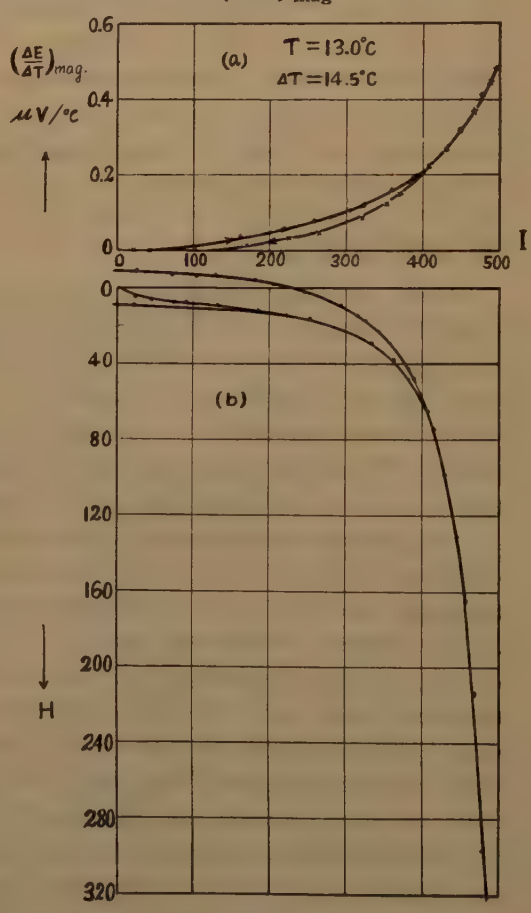


Fig. 1. (a) shows the magneto-thermoelectric powers with the magnetization and (b) shows the magnetization curves.

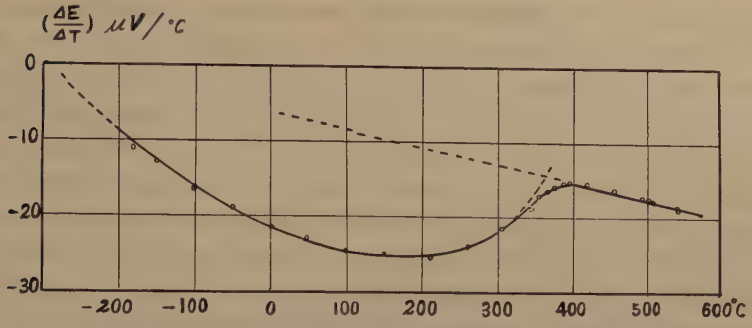


Fig. 2. The absolute thermoelectric power of nickel.

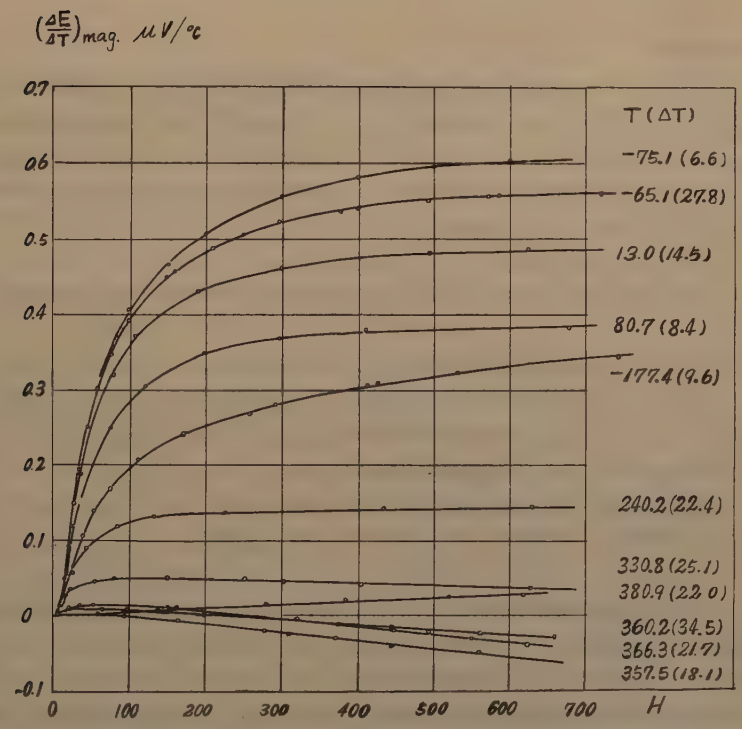


Fig. 3. Experimental relations between the magneto-thermoelectric powers and the magnetic fields at various temperatures.

magnetized one at cold junctions and the Fig. 1b is the magnetization curves of the specimen. We can not distinguish the differences among the kinds of the demagnetizing methods such as A.C. demagnetizing- and thermal demagnetizing- and other methods. The absolute thermoelectric powers of nickel on the temperature range between the boiling point of liquid oxygen and about 550°C are shown in Fig. 2, results of which are always negative.

Fig. 3 shows the functional relations between the magneto-thermoelectric powers on various temperatures and external magnetic fields. Fig. 4 shows the nearly saturated values quoted from the Fig. 3, where some corrections, as will be described immediately, are given to the values near the Curie point. We know from these results that (1) the magneto-thermoelectric power has a maximum value at about -90°C and decreases with decreasing temperatures and it may be true to tend to zero at the absolute temperature zero, and (2) there is a linear decreasing relation with increasing temperatures between the maximum point (-90°C) and near the Curie point, but (3) there appears a sudden decrease and shows a minimum negative value at the Curie point.

## § 3. Discussion

As pointed out in the previous papers the saturation values of magneto-thermoelectric powers are indefinite and are affected by the distributions of magnetic domains in a demagnetized state of the specimen. In our case, however, we may assume that there is no difference because the distributions of magnetic domains in demagnetized states are not so much affected, as described above, by the kind of demagnetizing methods on account of the some residual internal stress and comparatively small anisotropic energy constants.

We observe that the maximum saturation value of magneto-thermoelectric power appears at about -90°C as one of the authors has observed in the case of iron. It is reasonable that the maximum may appear at a certain temperature because the magneto-thermoelectric power must tend to zero at 0°K as was proved in the previous papers from the stand-point of the Nernst's heat theorem which states that the thermal e.m.f. must be zero at 0°K.

In the neighbourhood of the Curie point, since the additive magnetization proportional to the external field becomes more conspicuous than the magnetization due to the change of distribution of magnetic domains, the related phenomena such as magneto-resistance effect and magneto-caloric effect etc. must be distinguished from the effects which appear far below the Curie point. In our case, because the temperature gradient in the specimen may be changed by the magneto-caloric effect, the observed values of the magneto-thermoelectric power must be corrected by the measurement of temperature variation produced by this effect. Thus, for example, the linear part of the increasing of the magneto-thermoelectric power with the increasing magnetic fields as shown on the curve $T$=380.9°C $\Delta T$=22.0°C in the Fig. 3 can be explained as due entirely to the magneto-caloric effect from our measurement and some calculations. The relation between such corrected

values at $H$=570 Oerstead of the magneto-thermoelectric power and temperatures is shown in Fig. 4. Nevertheless, a negative deep valley appears

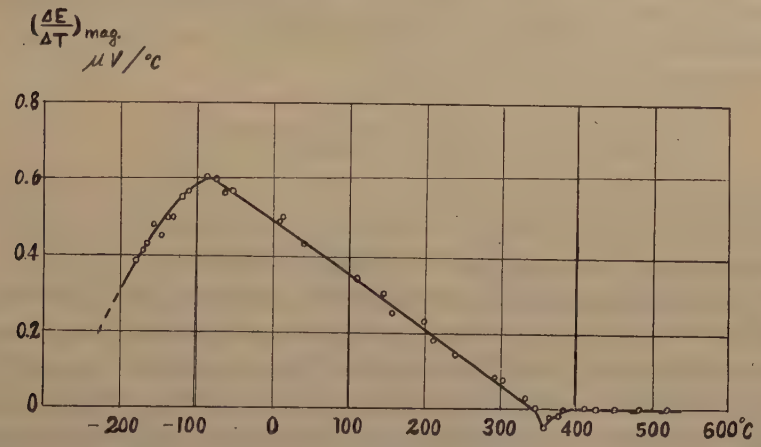


Fig. 4. The saturation values of the magneto-thermoelectric powers vis. temperature. The saturation values at low temperatures are obtained from the curves in the Fig. 3 by the extrapolation method and those in the neighbourhood of the Curie point are the corrected values at $H$=570 Oerstead.

in the neighbourhood of the Curie point, produced by the increasing additive magnetization expected from the Weiss' theory.

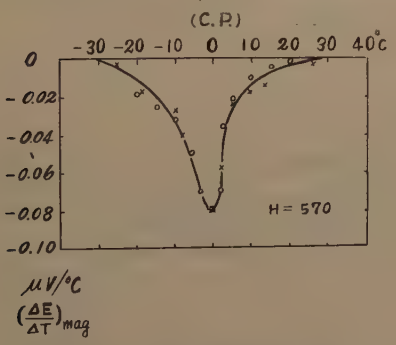


Fig. 5. The magneto-thermoelectric powers in the neighbourhood of the Curie point (C.P.). × and ○ in the figure show the magneto-resistance effect and magneto-caloric effect, respectively, indicated in suitable scales in order to coincide with the magneto-thermoelectric power at the Curie point.

Fig. 5 shows in more detail the magneto-thermoelectric powers in the neighbourhood of the Curie point with the magneto-caloric effect measured by us (○) and also with the magneto-resistance effect measured by Gerlach[2] (×) in suitable scales in order to coincide with the magneto-thermoelectric power at the Curie point. We know that from the coincidence of the effects these are caused by the similar origin, probably as mentioned above by the additive magnetizations proportional to the magnetic fields, and also that the decreasing of the absolute thermo-electric power by the appearance of magnetic domains below the Curie point as shown in the Fig. 2 corresponds to the decreasing of the magneto-thermoelectric power produced by the additive magnetization in the neighbourhood of the Curie point. If

we put that $\delta R$ and $\delta E$ are the change of the electric resistance and the thermoelectric power, respectively, by the appearance of spontaneous magnetization at 20°C just below the Curie point and $\Delta R$ and $\Delta E$ are the change of the corresponding quantities by $H=400$ Oerstead at the Curie point, then the next experimental values are obtained

$$\frac{\Delta R}{\delta R}=1.3\times10^{-2}, \qquad \frac{\Delta E}{\delta E}=1.2\times10^{-2}.$$

## § 4. Summary.

We summarize our experimental results as follows:

(1) The magneto-thermoelectric powers far below the Curie point are produced by the magnetization due to the change of distribution of magnetic domains and those in the neighbourhood of the Curie point are produced by the additive increasing magnetization proportional to the external field.

(2) At low temperatures both the magnetization and the magneto-thermoelectric power can not be easily saturated on account of the increasing of magnetic anisotropic energy constants.

(3) The magneto-thermoelectric power has the maximum value at about -90°C and then may tend to zero at 0°K. The linear relation between 0°C and 300°C coincides with that measured by Broili[3].

We are now measuring the magneto-thermoelectric power and magneto-striction of single crystal of nickel. The results, which are very interesting, and more detail discussions will be published recently in the Jour. Phys. Soc. of Japan.

## References

(1) Z. Funatogawa: Jour. Phys. Soc. Japan, 5 p. 311 (1950).
Z. Funatogawa: Jour. Phys. Soc. Japan, 6 p. 256 (1951).
Y. Gondo and Z. Funatogawa: Jour. Phys. Soc. Japan, 7 p. 589 (1952).
(2) W. Gerlach and K. Schneiderhan: Ann. d. Phys., 6 p. 772 (1930).
(3) H. Broili: Ann. d. Phys., 14 p. 259 (1932).

[Science Reports of the Yokohama National University, Sec. I, No. 3, 1952]

# Temperature Dependency of Magnetic Anisotropy of $Cd_3Mg$

By

**Nahonori MIYATA**

Alloys of Cd and Mg show intimate relations between their order-disorder transformations and magnetic properties as reported in the previous paper.[1] It is interesting for us to investigate their anisotropic characteristics by using the single crystals, since they have the hexagonal structures.

The experimental method was similar to what had been used by Rao and Sriraman for Cd and Zn.[2] A few results are shown in the figures, where $\chi_a$ and $\chi_c$ are the atomic susceptibilities along $a$- and $c$- axis of the crystals in the equilibrium states respectively and %'s mean the atomic concentrations of Mg. The anisotropic changes occured with the construction of the superlattices. For alloys which had excess Mg than $Cd_3Mg$ the two-steps changes appeared along both principal axes, but their features were quite different.

The temperature dependency of the mean values $\chi_{poly}=\frac{1}{3}(2\chi_a+\chi_c)$, which should give the character of the polycrystals, was in agreement with the previous investigation.[1]

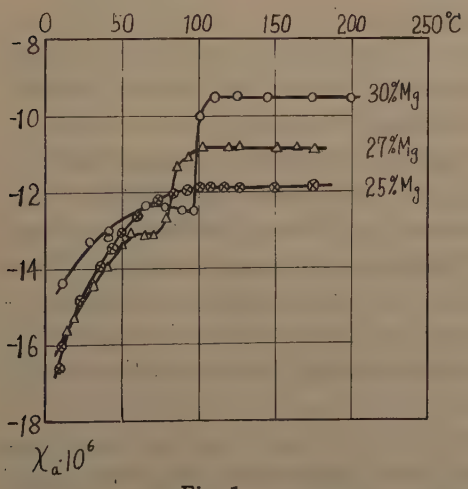


Fig. 1

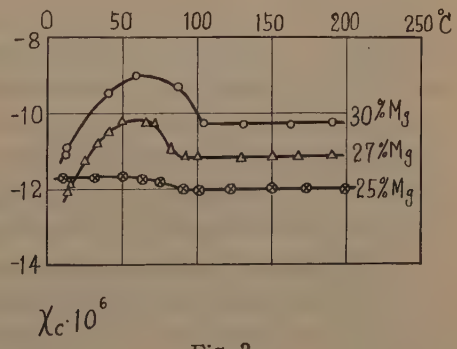


Fig. 2

## References

(1) N. Miyata: Science Reports of the Yokohama National University, Sec. 1, No. 1, p. 15 (1952)

(2) S. Ramachandra Rao and S. Sriraman: Proc. Roy. Soc. A. 166. p. 325 (1938)

[Science Reports of the Yokohama National University, Sec. I, No. 3, 1954]

# Study on Lichtenberg's Figures by Means of Color Films. (3rd Report).

By

**Bunji ARAI**

**Synopsis**

The background of Lichtenberg's figures obtained on color films was not colored black, but showed some color. What acted on the color film? The problem was investigated by the present writer, and it was found that these phenomena originated from the characteristics of color film of this country.

Some red streamers appeared often at tips of negative figures by color film. The writer considered that this fact would be due to the perpendicular construction on Lichtenberg's figures. To confirm this fact, experimentally, the writer obtained micro-photographs of section of streamer in Lichtenberg's figures by ordinary black and white film, and observed the distribution of silver particles in an emulsion layer at any parts.

## 1. Introduction

The background of Lichtenberg's figures obtained on ordinary films or dry plates by orthochromatic emulsion had no color and was transparent. But the background of Lichtenberg's figures obtained on color films by applying impulse, turned red over the whole film surface, as shown in Photo. 1. About this fact, the writer described already in former reports.[1] Now, even if the red fog is shut out by the black paper by using tungsten type, yet the background of figures appeared in dark olive green, as shown in Photo. 2-a, and by using sun light type dark violet, as shown in Photo. 2-b, which naturally should be black. The writer considered that the phenomenon was attributed to either of the action of strong electric field or character of color film. The judgement was made by the method to be described in next section.

The tips of negative figures obtained on color films in an ordinary position turned out usually red streamers. This fact seems to show that a red sensitive emulsion layer in the nearest celluloid base was excited by charged particles, as described in former reports.[1),2)] Then, he supposed that also in the case of black and white film, the silver particles at tips of a negative figure are in the nearest layer to celluloid base, as shown in Fig. 1.

Previously, C. E. Magnusson[3)] observed a slender prong of Lichtenberg's

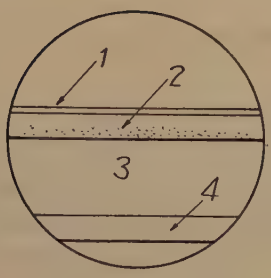


Fig. 1. Supposed diagram of section at tip of negative Lichtenberg's figure.

| No. | Name | Thickness |
|---|---|---|
| 1 | Protective gelatine film | 2 μ |
| 2 | Sensitive emulsion layer | 20 μ |
| 3 | Celluloid base | 100 μ |
| 4 | Antihalation layer | 15 μ |

figures by the microscope in perpendicular direction of surface of the dry plates. He described that "Visual examination of both the positive and negative figures by means of a compound microscope is more satisfactory, and that to study the microphotographs as for the higher magnification the thichness of the emulsion film is greater than can be observed without the change of focus. The dark specks are distributed through the emulsion film and not merely in a surface layer". The author researched directly the distribution of silver particles from the cross section of the sensitized film differing from Magnusson.

## 2. Experimental Apparatus for the Discrimination of Color in the Background

The connection for supplying the impulse to the films set in these cameras is shown in Fig. 2.

Through the experiments, the sphere spark-gap $G_1$ (2.5 cm $\phi$ brass ball) was used at 0.95 cm (30kV peak value, 25°C, 760 mm Hg.), the impulse applied by $G_1$ was chopped by the sphere gap $G_2$. $G_2$ (2.0 cm $\phi$ brass ball) was used at 0.60 cm (21.0kV peak value, 20°C, 760 mm Hg.).

These experiments were tried by the film of tungsten type only, because the cut film of sum light type was not prepared in market. For these experiments, *Fuji Color Cut Film* (tungsten type, non halation, safety base, Em. No. ATC–190–G) was used. The development of these color films was submitted to the Research Laboratory of the Fuji Photo-Film Co. Ltd.

For the glass plate in the special camera, the glass plate of dry plate was used. The glass plate was a cleared one which removed the emulsion. The thickness of this plate was 1.20 mm.

The metal plate in the special camera which was described in Fig. 2 of the former reports[2] was cut out from the half part, as shown in Fig. 3. There, the distribution of strength of electric field was varied from left to right. The colors of the parts left and right in the background of the figures obtained by the cameras were compared.

Also, the camera with the electrodes of point-ring arrangement was prepared, as shown in Fig. 4. The color inside the ring of the figures obtained in this camera was compared with that outside the ring.

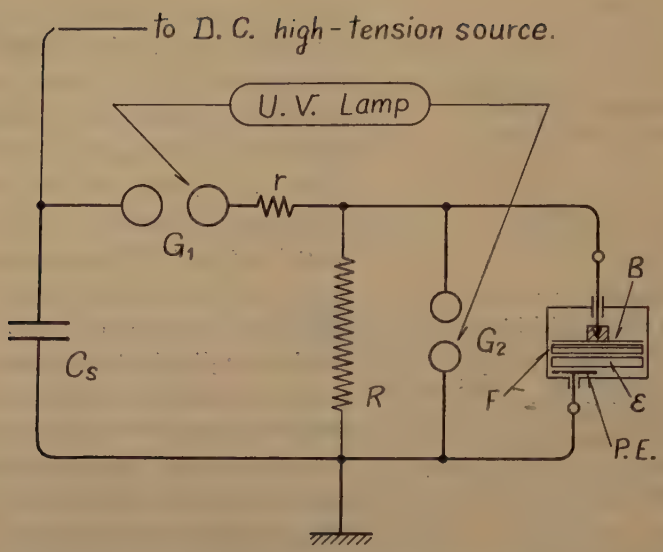


Fig. 2. Schematic connection diagram of impulse circuit to the special camera.

$G_1$ : Sphere spark-gap (2.5 cm $\phi$ brass ball, gap was fixed at 0.95 cm, 25°C, 760 mm Hg. 30kV max.).
$G_2$ : Sphere spark-gap for chopper of impulsive wave (2.0 cm $\phi$ brass ball), $G_2 < G_1$.
$G_S$ : Large Leyden Jar (0.0038 $\mu$F × 2).
r : Liquid resistance for damper of impulse (solution of $CuSO_4$ : 0.4KΩ).
R : Fixed resistance (HOKUOHM—resistance ready-made as a radio parts, 1MΩ × 10, $\frac{1}{2}$ watt type).
B : Black paper (cover of color film, 0.09 mm thick).
F : A group of sensitive emulsion layers of the color film.
ε : Glass plate (cleared by removing the emulsion of aged dry plate. 1.20 mm thick).
"*To D. C. high tension source*" leads to Gaiffe-Gallot et Pillon's apparatus.[1]

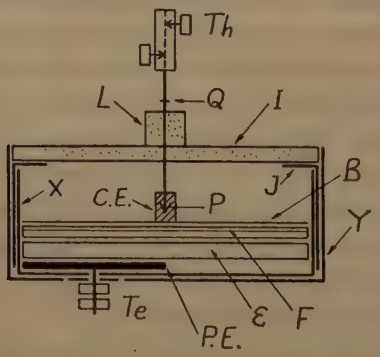


Fig. 3. Details of special camera designed for this experiment. Metal plate (P. E.) was cut out from the half part.

This camera was made by using an empty box of Agfa's Isochrom dry plates.
The whole surface of this camera was coated with bakelite varnish for keeping perfect insulation.

I : Bakelite plate (0.26 cm thick),
L : Bakelite lock nut. (1.0 cm $\phi$),
PQ : Copper threaded rod (0.20 cm $\phi$),
F : Color Film,
C. E. Brass cylindrical electrode (0.70 cm $\phi$) Threaded in P.
B : Black paper,
ε : Glass plate,
J. X. Y : Paper box. (size—10.8 cm × 8.3 cm × 1.9 cm),
Th : Terminal for high tension side.
Te : Terminal for earth side.

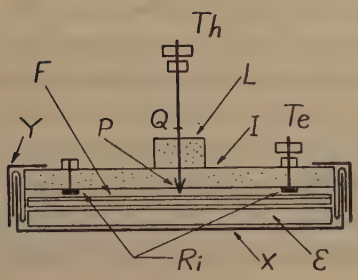


Fig. 4. Details of special camera with the electrodes of point-ring arrangement. The notation is the same at that for Fig. 3.
But, I: Ebonite plate (8.3 cm × 10.8 cm × 0.5 cm),
PQ: Brass rod electrode (0.30 cm $\phi$), Threaded in I and locked by L.
Ri : Brass ring electrode (Inside dia.—5.0 cm $\phi$, width—0.50 cm).

### 3. Results and Discussion for the Color of the Background

Photo. 3-a and 3-b show respectively the positive and negative figures obtained as shown in Fig. 3. In this case, no difference was found between the colors of left and right parts. Photo. 4-a and 4-b show the figures obtained by the cameras shown in Fig. 4, respectively. Photo. 4-a show the figure in which the center point was connected to the plus and the outside ring was connected to the minus (earth side). Photo. 4-b gives the inverse connection. In this case also, no difference in color was observed between the inside and outside.

In order to make sure this phenomenon, the writer observed the color of the film to which no impulse was supplied. There, no difference was recognized between the applied film and the not-applied one in the film of the same package. They were developed at the same time.

Then, the writer recognized that the colors of the background of Lichtenberg's figures which appear on the color films are the character of the color film in this country.

As seen in Fig. 7-a and 7-b, orange color appeared at the boundary of the metal plate. About this phenomenon, the writer thought that the red sensitive emulsion layer (deepest and nearest layer to celluloid base) and a part of green sensitive emulsion layer were excited by the strong electric field.

### 4. Sample and Präparat Making of the Section of Lichtenberg's Figures in Film

At first, the cut film (Fuji Portrait Pan.) was tried to be cut. But, it was difficult to cut a thin piece at uniform thickness. Its celluloid base was too thick (about 200 $\mu$) compared with an emulsion layer (20 $\mu$). Then, for this research, Roll Film (Fuji Neochrom Brownie, orthochromatic, F 120, non halation, Em. No. 021-D) was used, its celluloid base having a half thickness of cut film. The orthochromatic film was taken by reason of no necessity of the cover of black paper[1] to protect the fog over the whole film surface, and of easy dark room operation. This roll film was cut into about 10 cm

length. The emulsion of this film was put in an upper position, and was stuck on the glass plate by photo-paste at either end. The glass plate was a cleared one which removed the emulsion from the dry plate. These glass plates were 1.20–1.23 mm in thickness. After natural drying of the photo-paste and until perfect sticking in the dark room, it was put in the camera (as shown in Fig. 2 in former reports[2]). In order to apply the same crest voltage, to obtain clear and sharp positive and negative ordinary figures, and to apply the pulse at the same time on the films set in these cameras, the connection was arranged as shown in Fig. 5.

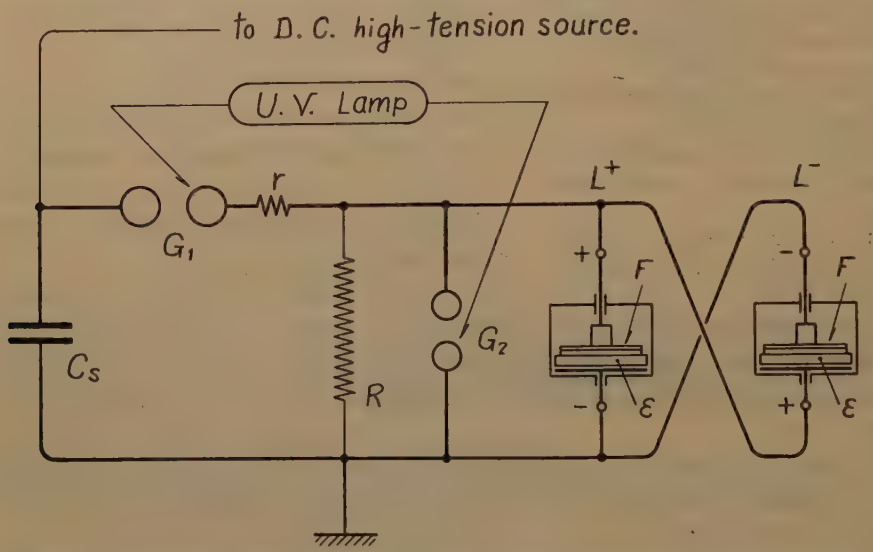


Fig. 5. Schematic diagram of the impulse circuit. Connection to these cameras, to apply the same crest impulse voltage, to obtain positive and negative figures at the same time. The notation is the same at that for Fig. 2.

See Photo. 5→8. From the emulsion layer of the film which was put in down position and stuck on the glass plate, unsharp inverese figures to positive and negative were obtained respectively as shown in Photo. 9, 10.

The writer picked up a typical streamer in these figures, and cut out strips including a streamer along other streamers from these films. Some samples of thin pieces were prepared by the following two method.

i) One of the method of ordinary botanical präparat making was taken. These strips were put in paraffin inbed (melting point: 52°C), and then the samples of thin pieces in the inbed were cut out as thinly as possible at the desired parts perpendicularly to the streamer by a safety razor blade with free hand. These thin pieces were put on a slide glass, and paraffin was removed by xylol. A temporary präparat was made by being soaked in xylol, under a cover glass.

ii) The other was a extemporaneously devised by the writer. The strip was inserted between two thick celluloid plates (about 3 mm thick), and its part desired to be cut was put at the end of the celluloid plate. These plates were pressed strongly and the part which bulged out of the strip was cut out by a safety razor blade with free hand. The end surface of the thick celluloid plate was used as the guide. Next, the strip was bulged out as the thickness of thin piece, and was cut in the same manner. These thin pieces were put on the slide glass and were soaked in a drop of water. The temporary präparat was preserved in this state, under the cover glass.

The samples were taken at the vicinity of the electrode, the intermediate of streamer, the tip, and the outside of tip.

## 5. Preliminary Discussion for the Sectional Distribution of the Specks in the Film of Lichtenberg's Figures

The numerical figures given at the side of microphotographs show the distance from the cylindrical electrode in mm.

Photo. 5, 6 show the series of micro-photographs by method i). The sample of ordinary positive figure near the electrode has a very dense distribution of the specks as shown in Photo. 5-0, and in other samples these specks distributed in the upper layer of emulsion. In the ordinary negative figure, the same distribution as that of positive figure was observed near the electrode, as shown in Photo. 6-0. But in the tip, these specks distributed in the lower layer of emulsion nearest to the celluloid base.

The series of micro-photographs by method ii) are shown in Photo. 7→10. Photo. 7, 8 show ordinary positive and negative figures, Photo. 9, 10 show inverse positive and negative figures respectively.

The distribution of specks in the lower layer near the celluloid base was observed clearly in the sample of the unsharp streamer in Photo. 7-11.5. This fact corresponds to the unsharp red streamer in the color film in former reports[1),2)]. But in Photo. 8, the tendency as seen in Photo. 6 was not observed. Because all tips have not been observed, the above description cannot be insisted.

In any case, the color distribution of streamers obtained by the color films as shown in Fig. 4, 6, 8, 10 of former reports[2)] are explained by the vertical distribution of the specks obtained here. In Photo. 9, 10 the samples near the electrode have the dense speck distribution over the whole range from the lower to upper emulsion layer. In the tips, the specks distributed at the lower layer only far from the celluloid base. These coincide with the color figure as shown in Fig. 5, 7, 9, 11 of former reports.[2)] For comparison, Photo. 11 shows the micro-photographs of the section of films by ordinary light.

From the above observation, the writer considered that Lichtenberg's figures have vertical construction.

This report is a summary of the lecture made at the Special Meeting on Discharge Physics, held by the Physical Society of Japan, Oct., 16. 1953.

In conclusion, the writer wishes to express his hearty thanks to Dr. U. NAKAYA, Dr. C. MAGONO, Dr. T. ASAHINA (National Science Museum) and Dr. S. FUJISAWA (Director of Fuji Photo-Film Research Laboratory) who made suggestions to him throughout this work.

The writer is also indebted to Assistant Prof. S. NAGAMI (The Botanical Dep.) for präparat making, and to Mr. T. ONO (Tokyo Sibaura Electric Works Co. Ltd.) for his supply of materials etc. in this research.

Oct., 29. 1953.

## References

1) B. ARAI: "Study on Lichtenberg's figures by Means of Color Films"., Science Report of the Yokohama National University, Sec. I. No. 1. pp. 27-38: March, 1952.
2) B. ARAI: "Study on Lichtenberg's figures by Means of Color Films. (2nd Report)"., Science Report of the Yokohama National University, Sec. I. No. 2. pp. 41-46: March, 1953.
3) C. E. MAGNUSSON: "Lichtenberg Figures"., A. I. E. E. pp. 828-835, XLVII, 1928.

Photo. 10→15.

Micro-photographs show cross sections perpendiculaly to streamers. Numerical figures written at the side of microphoto. show the distance (in mm) from the cylindrical electrode. Scale of min. devision show 10 μ.

Photo. 10, 11:

Sample: Paraffin inbed, soaked in xylol,
Microscope and Camera: YASHIMA (×150)—Hand made camera (×75).

Photo. 12→15:

Sample: Soaked in water,
Microscope and Camera: WINKEL (×154)—Canon (×45).

Data of lichtenberg's figures shown in Fig. 10→15

Data and Time: Sept. 23. 1953, 12h45m→14h45m.
weather: Rain, Room Temp.: 22.6°C,
Atom. Press. (mm Hg): 762.6→761.9, Humidity (%): 75→76.
$G_1$: 0.95 cm (30 kV), $G_2$: 0.50 cm (18.0 kV), $C_S$: 0.0038μF×2, r: 0.4 kΩ, R: $10^7$Ω.

Photo. 5. Ordinary positive figure (×1.5) and its microphotographs (×175) at cross section of streamer (×2.5).

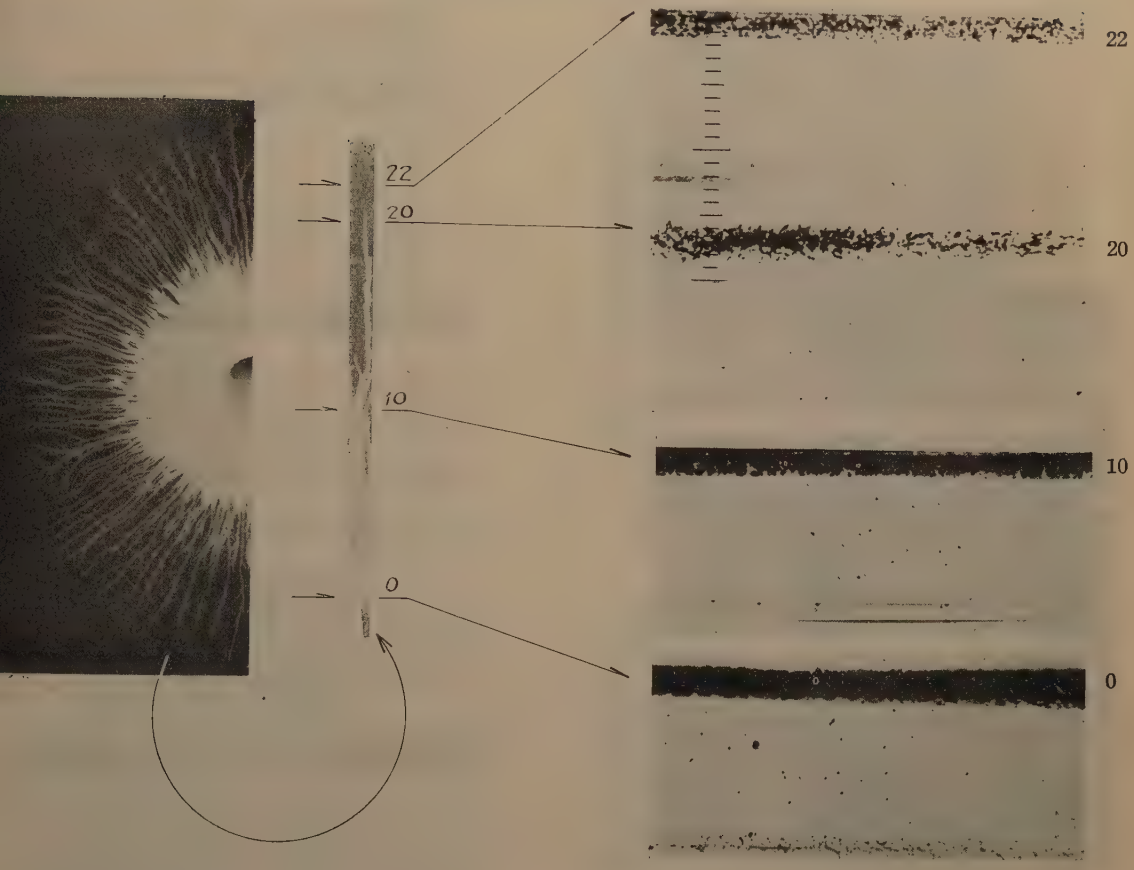

Photo. 6. Ordinary negative figure (×2.5) and its microphotographs (×175) at cross section of streamer.

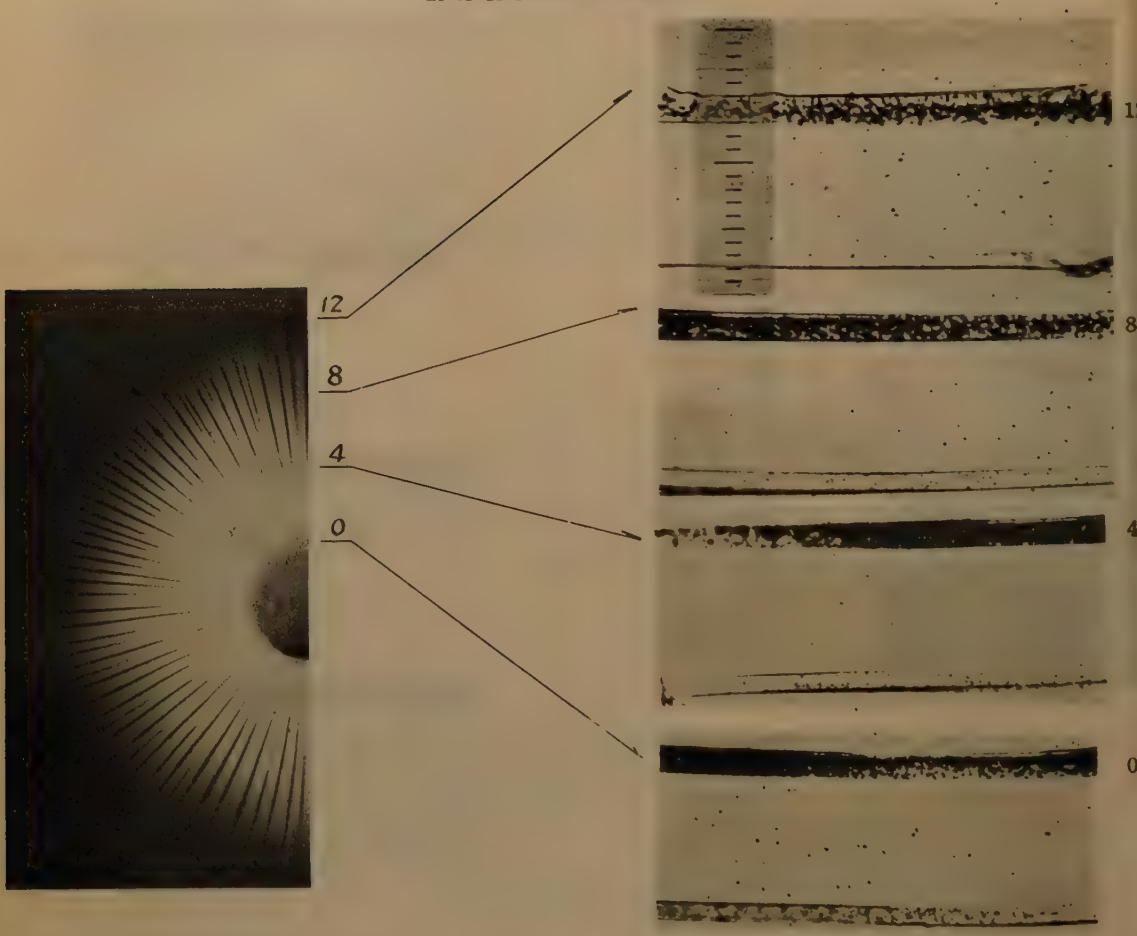

Photo. 7. Ordinary positive figure and its microphotographs at cross section of streamer.

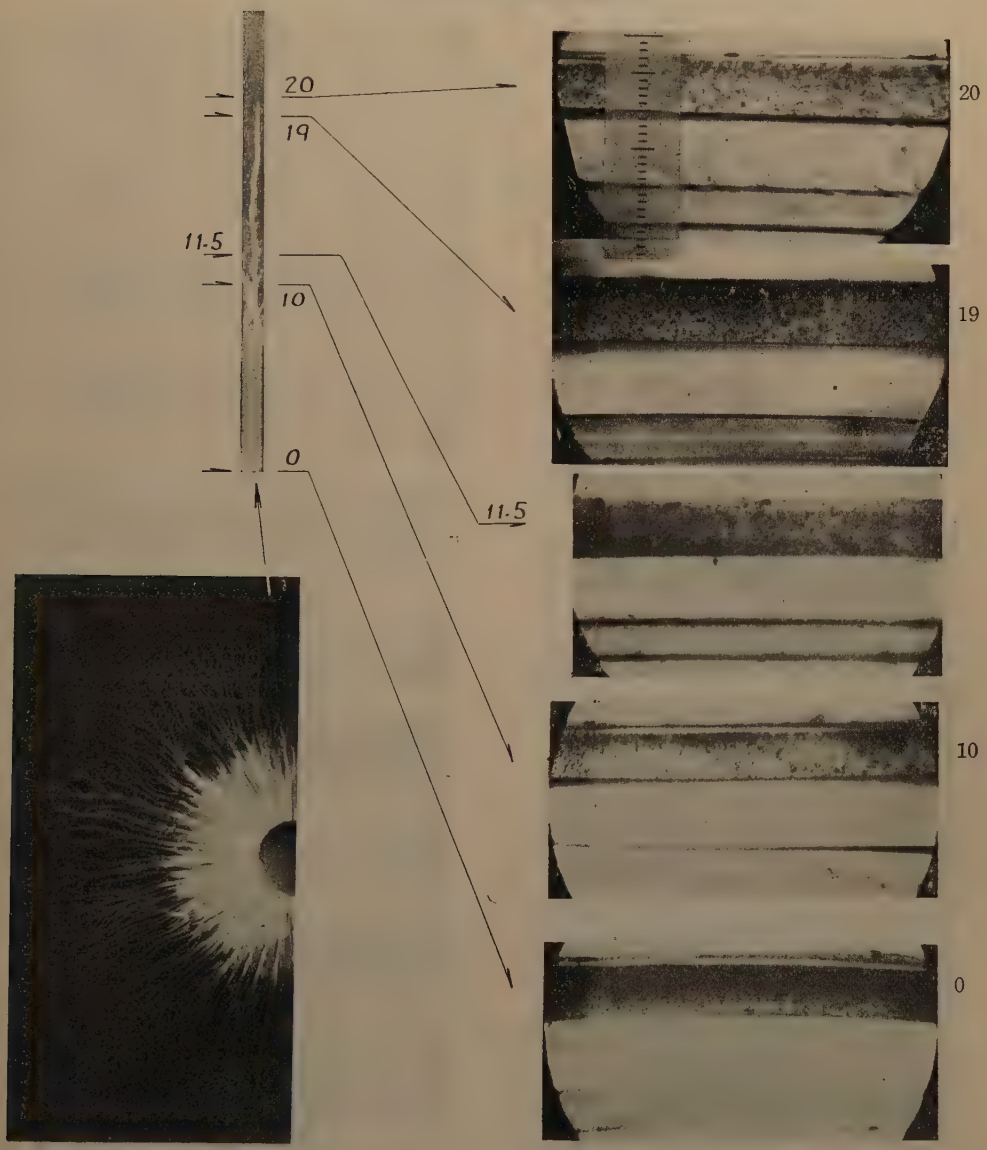

Photo. 8. Ordinary negative figure and its microphotographs at cross section of streamer.

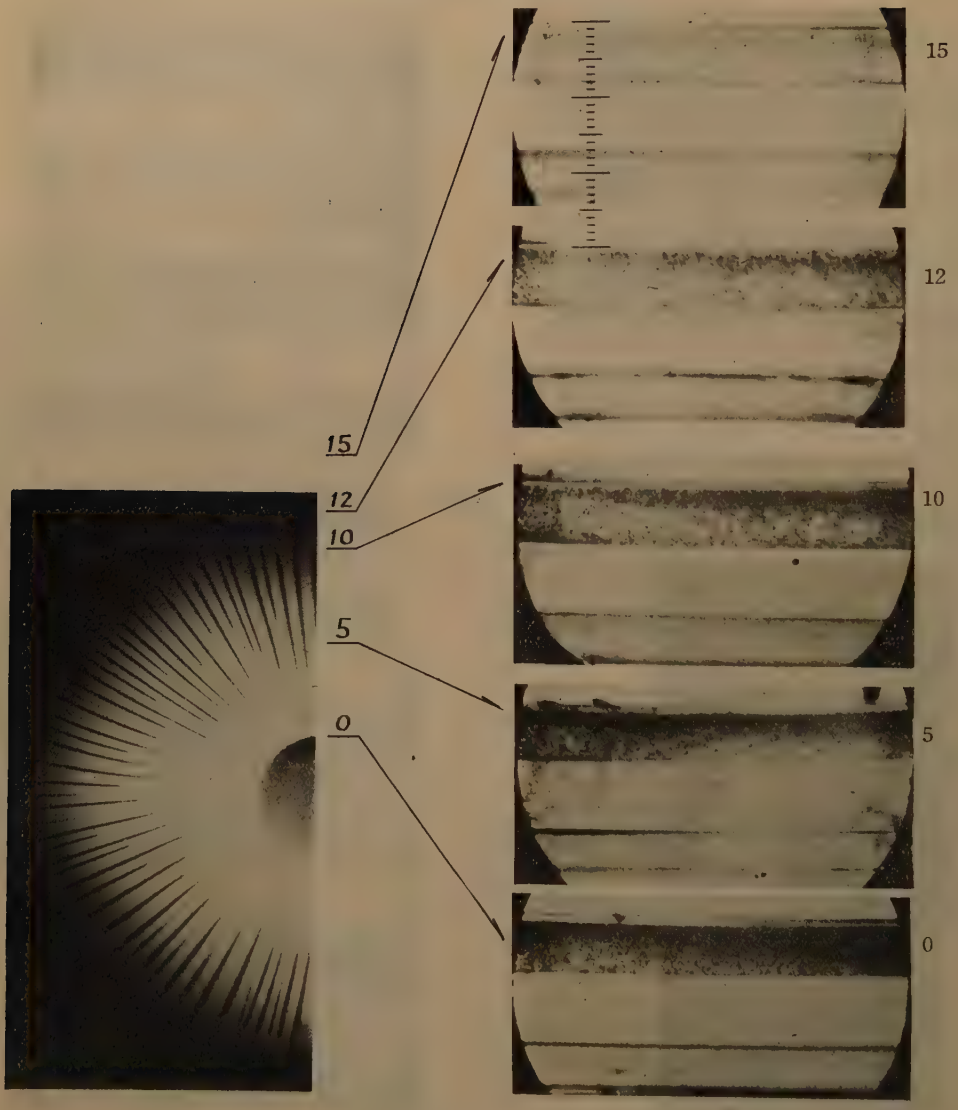

Photo. 9. Inverse positive figure and its microphotographs at cross section of streamer.

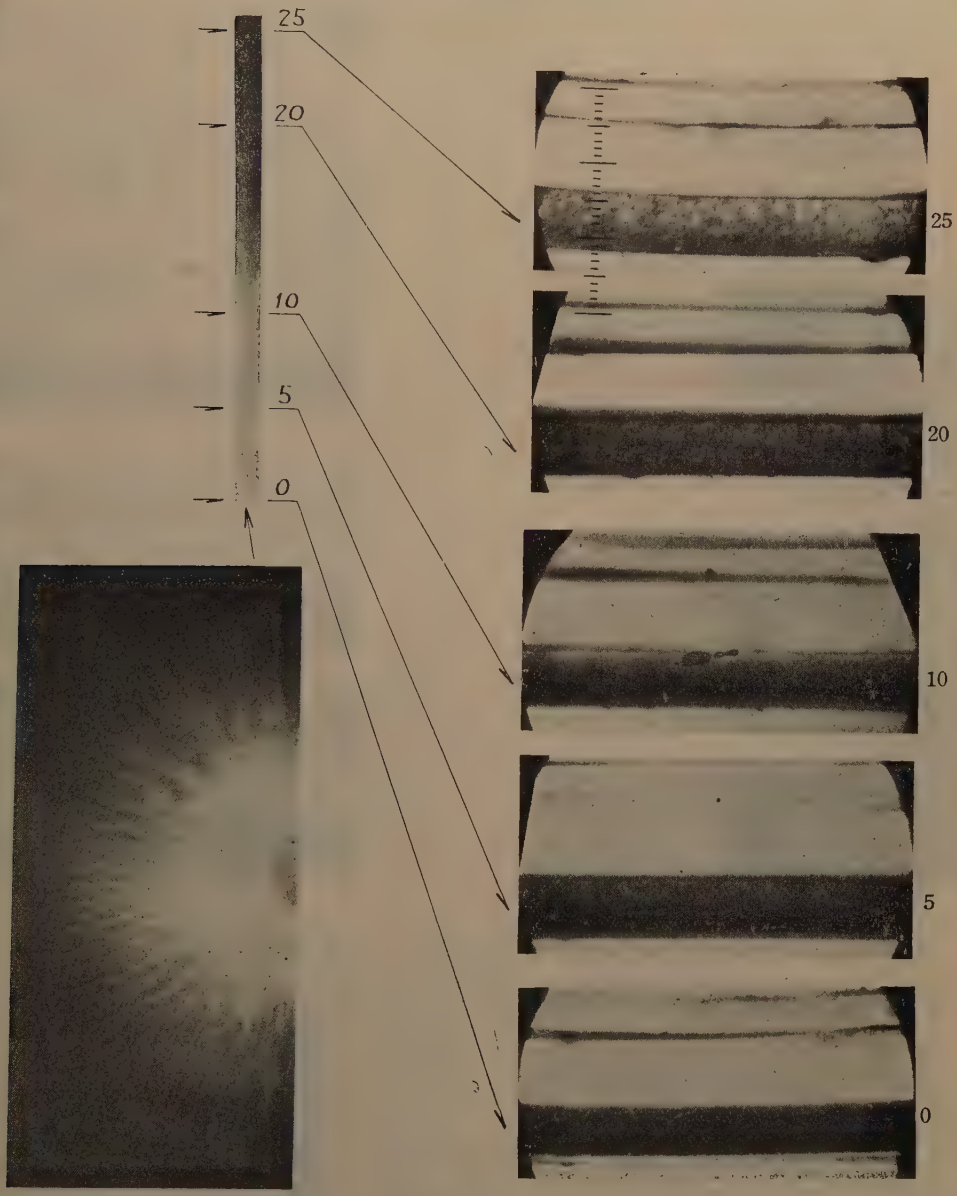

Photo. 10. Inverse negative figure and its microphotographs at cross section of streamer.

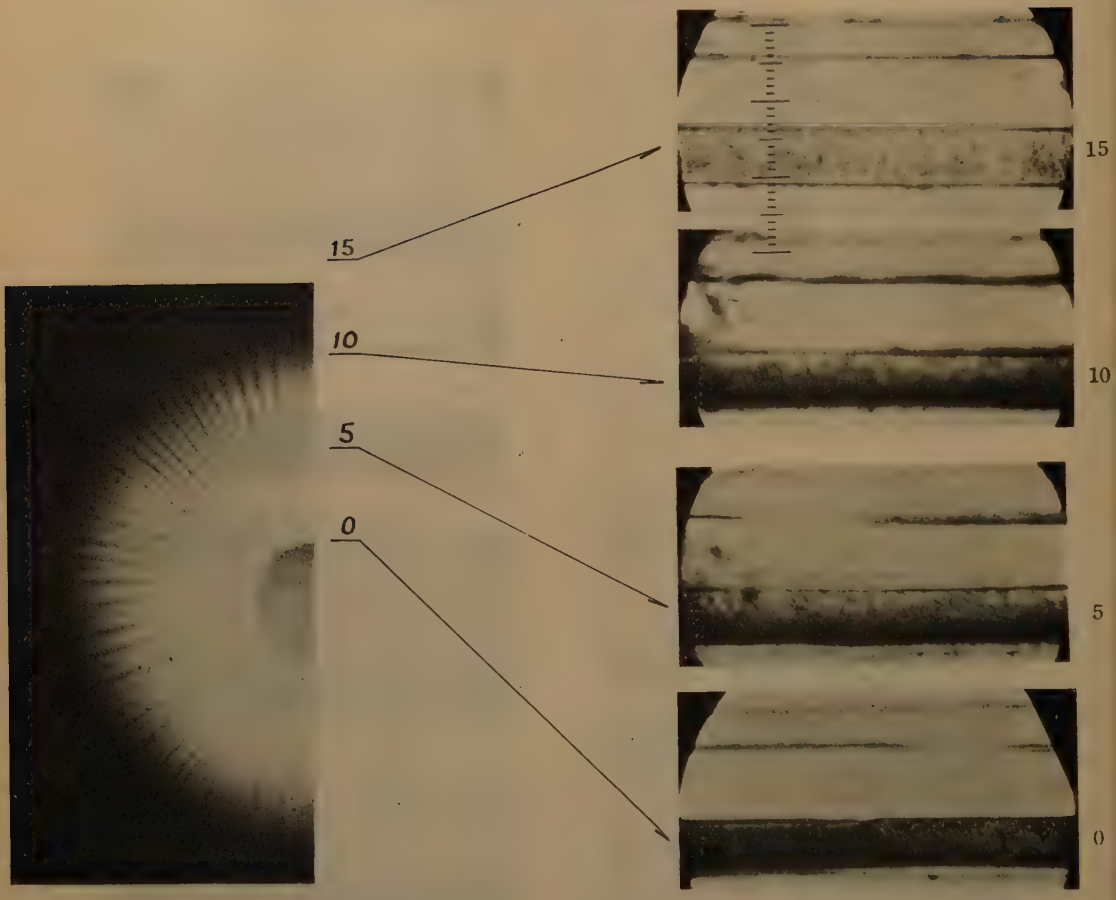


Photo. 11. Micro-photograph at section of sensitized film by ordinary light. Neumerical figures show the notation, they are the same at that for Fig. 1

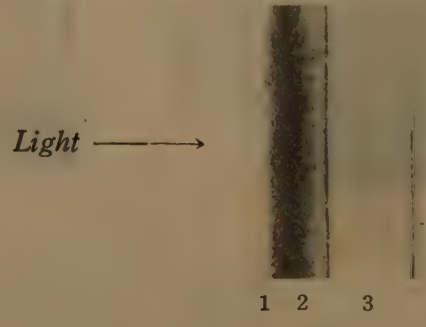

Photo. 1.: Positive and negative Lichtenberg's figures (15.6 kV) obtained on color films, whole film surface turned red.

Photo. 2–a.: Lichtenberg's figures (21.0 kV) obtained on tungsten type color film, the background appears dark olive green.

Photo. 2-b.: Sunlight type (14.8 kV). Both figures shows inverse negative one.

Photo. 3–a, 3–b: Positive (dendritic) and negative (tertially) figures (21.0 kV) obtained as shown in Fig. 3. Compare the colors of the parts left and right in background of the figures.

Photo. 4–a: Center point was connected to the plus high-tension terminal (21.0 kV), and outside ring was connected to the earth.

Photo. 4–b: Inverse connection of Photo. 4–a. Both figures obtained by the camera shown in Fig. 4.

Photo. 1. (+&−), naked.

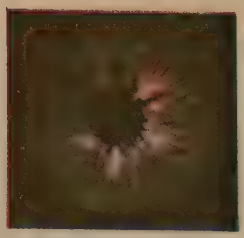

Photo. 2-a. (−).

Photo. 2-b. (−).

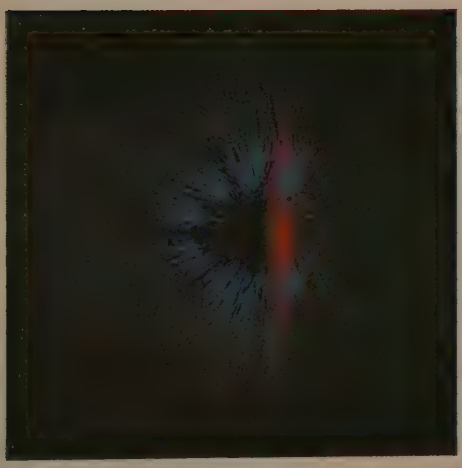

Photo. 3-a. (+).

Photo. 3-b. (−).

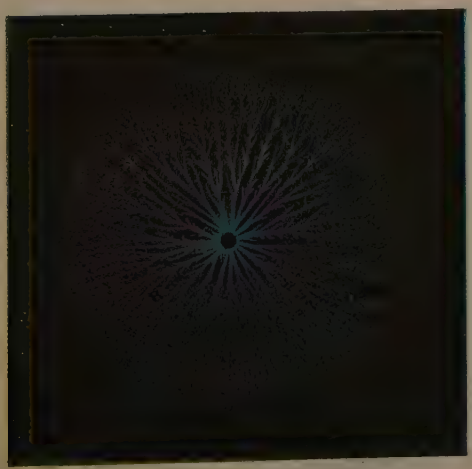

Photo. 4-a. (P: +, R: −), naked.

Photo. 4-b. (P: −, R: +), naked.

Photo. by B. Arai

[Science Reports of the Yokohama National University, Sec. I, No. 3, 1954]

# On the Falling Velocity of Solid Precipitation Elements

By

Chōji MAGONO

**Abstract**

Falling velocity of various solid precipitation elements was discussed theoretically, and simple relations between the dimension, the density, and the falling velocity were derived, utilizing well known aerodynamic principles and constants.

## Introduction

It is considered that almost all rain drops originate from solid precipitation elements, and the rates of growth of these elements depend on their falling velocities. So the falling velocity seems to be one of the most important problems in the investigation of the mechanism of the precipitation phenomena. Since prof. Nakaya[1] observed the falling velocity of snow crystals, no discussion has been done for the falling velocity of solid precipitation. To calculate the rate of growth of snow precipitation, it is desirable to formulate the falling velocity of various precipitation elements by their dimensions. To discuss the falling velocity theoretically, it is necessary to know their falling states and their densities during the fall. The author observed the solid precipitation elements in their falling states by a stroboscopic camera[2], but their densities were then not measured. During recent two seasons, many measurements of the density of various snow flakes were made by the photographic method[3], and the theoretical discussion became possible. It is the purpose of this work to search the relation between the falling velocity of solid precipitation, utilizing the aerodynamic principles.

## § I. Falling velocity of snow crystal of plane type

a) *Dendritic snow crystal.*

In the previous report[2], it is ascertained that the snow crystal of plane type falls keeping its plane horizontally. When the snow has reached its terminal velocity $u$, its weight is balanced by the air drag,

$$sh(\sigma-\rho)g = C_p s \frac{1}{2} \rho u^2, \qquad (1)$$

where $s$ is the area of its horizontal cross-section, $h$ its thickness, $\sigma$ its density, $\rho$ the density of air, $g$ the gravitational acceleration, and $C_p$ is the drag coefficient of the circular plate. Thus

$$u=\sqrt{\frac{2h(\sigma-\rho)}{C_p\rho}g}. \qquad (2)$$

From Nakaya's observation, the thickness of this type was nearly 0.0011 cm, being independent of the dimension. $\sigma$ is considered to be 0.9 g cm$^{-3}$. $C_p$ is assumed here to be 1.2, (Reynolds' number* $10^2$~$10^3$). This assumption is consistent with Dr. Spilhaus' paper.[4] On the assumption, the terminal velocity of dendritic crystal of plane type was calculated from (2),

$$u=35\,\text{cm sec}^{-1},$$

which indicates that the velocity of plane dendritic crystal is independent of its dimension as Nakaya had pointed out[1]. And this value agrees fairly with the observed data as shown in Fig. 1. The difference between the value observed and calculated may be due to the estimation of $C_p$, partially to the fluttering motion of the snow crystal in falling state.

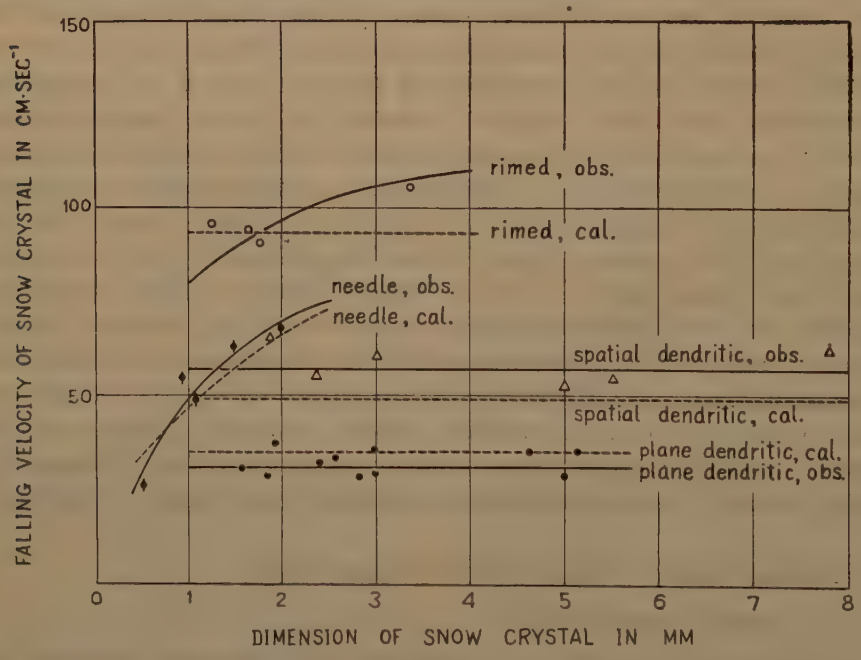


Fig. 1

* Strictly speaking, it is impossible to select $C_p$ unless the falling velocity is known, because the drag coefficient varies with Reynolds' number. In this paper, the falling velocity of snow crystals requisite for calculating Reynolds' number were temporarily assumed to be 1 m sec$^{-1}$.

b) *Rimed crystal.*

Because no observation has been made for the density of rimed crystal, it is difficult to estimate the thickness and the density requisite for calculating formula (2). Nakaya gave following formulae for individual mass of crystal,

for plane dendritic crystal $m = 0.00038\, d^3$, (3)

for rimed crystal $m = 0.0027\, d^2$, (3′)

where $m$ is the mass of the crystals in g, $d$ the diameter of the crystal in cm. The author considered that the thickness of the rimed crystal observed by Nakaya was proportional to its mass, therefore, using (3) and (3′) $h$ is given,

$$h = 0.0011 \times \frac{0.00038\, d^2}{0.0027\, d^2} = 0.0079 \text{ cm}.$$

In this case also, $\sigma$ is equalized to $0.9\,\text{g cm}^{-3}$, for the thickness calculated here is equivalent to a compact ice plate. Thus the falling velocity of rimed crystals was acquired from (2),

$$u = 94 \text{ cm sec}^{-1},$$

being independent of their dimensions as shown in Fig. 1. One may see that the observed values of rimed crystals tend to increase with their dimensions. The disagreement between the values observed and calculated is perhaps due to the experimental formula (3′), in which the mass of rimed crystal is regarded as proportional to its area, being independent of its dimension. More numerous observations for the rimed crystals are desirable.

## § 3. Falling velocity of snow crystal of spatial type.

In this case also, the difficulty in the estimation of $h$ and $\sigma$ is not avoided, but the formula (2) may be approximately deformed as follows,

$$u = \sqrt{\frac{2h(\sigma-\rho)}{C_D \rho} g} \fallingdotseq \sqrt{\frac{2h\sigma}{C_D \rho} g}. \qquad (4)$$

Assuming that the shape of spacial crystal is a circular cylinder as shown in Fig. 2, the volume is calculated,

$$\text{volume} = \frac{\pi}{4} d^2 h,$$

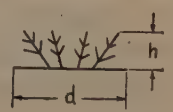

Fig. 2. Side view of spatial snow crystal.

where $d$ is the diameter of the base plane, $h$ the height. In Nakaya's paper, the mass of the crystal of this type is described as following formula,

$$m = 0.0010\, d^2$$

Thus the density is determined.

$$\sigma = \frac{m}{v} = \frac{0.0040}{\pi} h, \qquad (5)$$

where $v$ is the volume. Using the density,

$$u=\sqrt{\frac{0.008}{C_p\pi\rho}g}=49 \text{ cm sec}^{-1},$$

which indicates that the falling velocity of spatial type is also independent of its dimension. As seen in Fig. 1, the value calculated here is a little smaller than observed one. This disagreement may be due to the estimation $C_p$: 1.2. Because the thickness of spatial crystal is comparable with its base dimension, $C_p$ must be selected smaller than 1.2 probably.

## § 4. Falling velocity of snow crystal of needle type.

By means of the stroboscopic camera, it was observed that the snow crystal of needle type falls keeping its long axis horizontally. When the crystal has reached its terminal velocity $u$, its weight is balanced by the air drag which is perpendicular to the side plane of the needle, thus,

$$\frac{\pi}{4}d^2 l(\sigma-\rho)g=C_c\, d\, l\,\frac{1}{2}\rho u^2, \qquad (6)$$

where $d$ is the diameter of needle, $l$ the length, $C_c$ the drag coefficient of the circular cylinder.

Thus,

$$u=\sqrt{\frac{\pi d(\sigma-\rho)}{2C_c\rho}g}. \qquad (7)$$

Calculating the masses for six samples of needle type in Nakaya's book[5], it was found that their densities were about 0.15 g cm$^{-3}$, being independent of their lengths. And plotting the diameters of the needles shown in the book to the length as seen in Fig. 3, following relation was found,

$$d=0.08\, l^{*}.$$

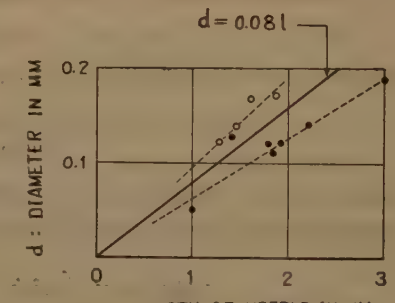

Fig. 3

From the result of the experiment by the wind tunnel[6], it is known that the drag coefficient of circular cylinder set vertically to wind is about 0.7 in the range of Reynolds' number $10^2\sim10^3$, $\frac{l}{d}=\infty$. Therefore (7) is rewritten as follows,

$$u=1.4\times10^2\sqrt{l} \text{ cm sec}^{-1}.$$

The falling velocity calculated thus, is plotted together with the observed values in Fig. 1. With the agreement of this order, we should be satisfied in this case.

* Dr. Houghton[7] assumed $d=0.1\sim0.075\, l$.

## §5. Falling velocity of graupel.

By means of the stroboscopic camera, and from the Author's observation of graupels fallen on a mire, it was ascertained that the graupel of cone type falls keeping its top upward, and as well known, its bottom is approximately hemispherical. So, it will be accepted that the drag coefficient of the sphere was adopted to calculate the falling velocity of the graupel. In the terminal state, the weight of the graupel is balanced by the air drag,

$$\frac{\pi}{6} d^3(\sigma-\rho)g = C_s \frac{\pi}{4} d^2 \frac{1}{2} \rho u^2, \tag{8}$$

where $d$ is the diameter, $\sigma$ the density, and $C_s$ the drag coefficient of the sphere. Thus we obtain

$$u = \sqrt{\frac{4}{3} \frac{d(\sigma-\rho)}{C_s \rho} g}. \tag{9}$$

The drag coefficient of sphere varies with Reynolds' number, but the falling velocity of the graupel is yet unknown in this case. To simplify the calculation, the value of drag coefficient: 0.5 was adopted according to Newton's estimation. As for the value, it will be later described in detail. Thus the terminal velocity $u$ is described by the function of the diameter and density only. In Fig. 4, $u$ is plotted by broken lines as the function of $d$ with parameter $\sigma$. As shown by the dots in Fig. 4, the falling velocities observed by Nakaya, situate between the densities 0.12 and 0.14 g cm$^{-3}$. Considering that Nakaya gave 0.125 g cm$^{-3}$ as the mean density of the graupels, it is accepted that the falling velocity of graupel is well described by (9), except the smaller range. In the range smaller than 2 mm, the observed values are relatively small. This difference may be due to the assumption that the drag coefficient is constantly 0.5 even in such a small Reynolds' number $2\times10^2$. By the measurement of Dr. Gunn[8], the drag coefficient of the water drop in these Reynolds' number is about 0.7. It appeas that if the increase of drag coefficient with the decrease of Reynolds' number is considered, the difference will decrease. On the other hand, the effect of scattering of the density should not be neglected. As shown in Fig. 5, it is

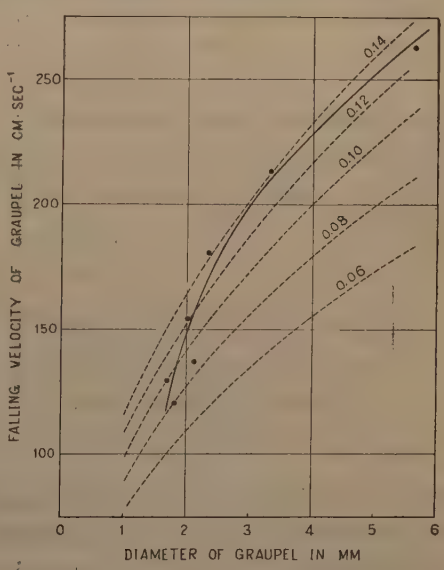

Fig. 4

apparent that the larger the graupel, the larger the density. To discuss the falling velocity in detail, it is necessary the simultaneous measurement of the density and the falling velocity of individual graupels.

## § 6 Falling velocity of snow flake.

In the previous report[2], the author described that the snow flake receives the resistance proportional not only to its horizontal cross-section, but to its volume. There, the falling velocity was derived from following equation,

$$\frac{4}{3}\pi r^3(\sigma-\rho)g=(A\pi r^2+B\pi r^3)\frac{1}{2}\rho u^2, \qquad (10)$$

where $r$ is the radius of snow flake of spherical type. The constants $A$, $B$ adopted in the report, were inadequate.

It may be natural to consider that $B$ is the function of the density of the snow flake, because the term $Br^3$ shows the resistance by a part of air which passes through the snow flake. In order to determine the function, the density of the graupel through which air can not pass, was considered. The minimum density of graupel observed hitherto, is about 0.05 g cm$^{-3}$ as shown in Fig. 5. Therefore, it is reasonable that $B$ is proportional to $(0.05-\sigma)$ g cm$^{-3}$, that is, $B=(0.05-\sigma)y$. In the case of non-permeable spherical body, the drag coefficient is estimated to be 0.5 as descrived above. (Reynolds' number $10^3\sim10^4$). So $A$ was considered to be described by following formula,

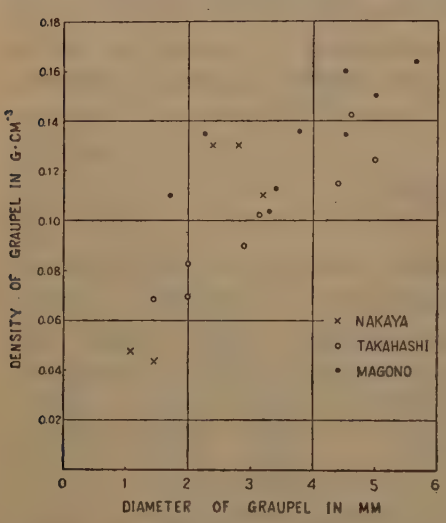

Fig. 5

$$A=0.5-(0.05-\sigma)x,$$

where $x$ and $y$ are constants of no dimension. To determine those constants by the results of observations and formula (10), the simultaneous observations of the density, the radius, and the falling velocity are necessary. But no simultaneous observation has been made for those elements. During recent two seasons, the author measured the density of various snow flakes. Their volumes and diameters in falling state were determined by the "photographic paper method"[3], and their masses were determined by the increase of the weight of the photographic paper by falling of the snow flakes. The results are plotted in Fig. 6. One may see there the tendency that the larger the diameter, the smaller the density. This tendency appears to originate from

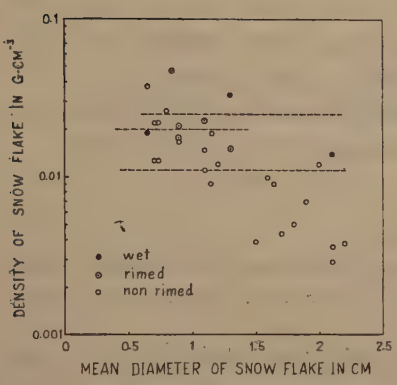


Fig. 6

the fault of the photographic paper method, in which the volumes of all snow flakes are calculated from the traces coloured on a photographic paper, neglecting that the large snow flakes do not always take a spherical form but often oblate ones. From Fig. 6, the mean density of rimed snow flakes for which many observations had been made, was temporarily assumed to be 0.02 g cm$^{-3}$. Besides the density, two mean falling velocities 195 cm sec$^{-1}$ and 208 cm sec$^{-1}$ of oblate and prolate type at the diameter 2 cm and 3 cm, were adopted to determine $x$ and $y$. Introducing these values to (10), the constants $x$ and $y$ were calculated,

$$x=3, \quad y=20.$$

Thus the falling velocity of snow flakes was semi-theoretically acquired,

$$u=\sqrt{\frac{8}{3}\frac{\sigma-\rho}{\rho}\frac{r}{0.35-3\sigma+(1-20\sigma)r}g} \tag{11}$$

Assuming that tha densities of the non-rimed snow flake and wet snow flake were 0.011 and 0.025 g cm$^{-3}$ respectively, the formula (10) describes their falling velocities as shown in Fig. 7. In the figure, one may see that these

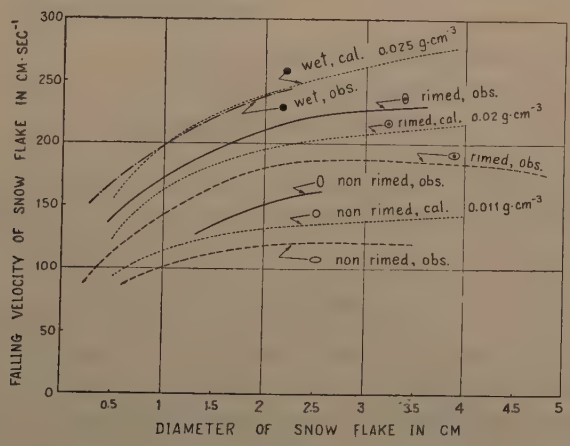


Fig. 7

calculated values of spherical type place half way of those prolate and oblate type in the wide range. Considering the density shown in Fig. 6, it may be accepted that the assumptions descrived above were not so unreasonable.

More simultaneous observations of the size, density, and falling velocity of snow flakes are desired to dicuss the falling velocity more exactly.

In conclusion, the author wishes to express his best thanks to Prof. U. Nakaya whose observation occupies the essential part in this work, and to Mr. T. Maruo who gave the author useful advices in the aerodynamics.

## References

1) Nakaya, U. and T. Terada, Jr., 1935: Simultaneous observations of the mass, falling velocity and form of individual snow crystals. J. Fac. Soc., Hokkaido Imp. Univ., Ser. II, 1, 191~200.
2) Magono, C., 1953: On the growth of snow flake and graupel. Sci. Rep., Yokohama Nat. Uni., Sec. I, No. 2, 18~40.
3) Magono, C., 1954: Investigation of the size distribution of precipitation elements by the photographic paper method. Of this Journal 41~53.
4) Spilhaus, A. F., 1948: Rain drop size, shape, and falling speed. J. Met., 5, No. 3, 108~110.
5) Nakaya, U., 1949: Investigation of snow (in Japanese), Iwanami, Photos. 1034~1039.
6) Wieselsberger, C., 1932: Handbuch der Experimental-physik, 4, 2. Teil, 312, A. V. M. B. H., Leipzig.
7) Houghton, H. G., 1950: A preliminary quantitative analysis of precipitation mechanism. J. Met., 7, 363~369.
8) Gunn, R. and G. D. Kinzer, 1949: The terminal velocity of fall for water droplet in stagnant air. J. Met. 6, 243~248.

[Science Reports of the Yokohama National University, Sec. I, No. 3, 1954]

# Investigation of the Size Distribution of Precipitation Elements by the Photographic Paper Method

By

**Chōji MAGONO**

**Abstract**

It is considered that the size distribution of solid precipitation is more important than that of rain drop to investigate the mechanism of precipitation. In this work, the relation between the diameter of various precipitation elements and the records coloured by them on the photographic paper, was mainly investigated.

a) *Rain drop.*

From the calibration of the water drops at terminal velocity, the following relation was obtained,

$$d = 10^{-\frac{1}{2}} D^{\frac{2}{3}},$$

where $d$ = diameter of rain drop in mm, $D$ = mean diameter of wet area by rain drop on the photographic paper in mm.

b) *Snow flake and snow crystal.*

The outline of the horizontal shape of snow flake or snow crystal in falling state is coloured and recorded on the photographic paper, so we obtain

$$d = 2^{-\frac{1}{2}} D,$$

where $d$ = mean diameter of snow flake or snow crystal assumed to be ellipsoidal in falling state, $D$ = mean diameter of area coloured on the photographic paper in mm.

c) *Very wet or partially melted snow flake.*

Very wet or partially melted snow flakes collapse and spread on the photographic paper when they fall on it. Their thicknesses are roughly uniform, so their diameters in falling state are calculated from their records on the paper and their uniform thickness

$$d = (1.5)^{\frac{1}{3}} h^{\frac{1}{3}} D^{\frac{2}{3}},$$

where $d$ = diameter, $h$ = thickness of snow flake and $D$ = mean diameter of coloured area in mm.

d) *Graupel.*

The graupel melts to a hemispherical drop on the paper, so its diameter equivalent to that of a spherical water drop is calculated as follows,

$$d_\omega = 2^{-\frac{1}{3}} D',$$

where $d_\omega$ = equivalent diameter, $D'$ = diameter of dark brown area in mm.

Some examples of the traces by various precipitations on the photographic papers and their size distributions are shown in some photographs and figures.

## Introduction

The size distribution of precipitation elements gives us an important method to search the mechanism of precipitation, and to use the result of a radar echo. While, except the rain drops no attempt has been made to observe the size distribution of other solid precipitation. It is not impossible to observe the mass distribution of solid precipitation by the "filter paper method" like the rain drop, but in the case of solid precipitation, the simultaneous observation of its sort and size is also desirable. Specially, in the sleety weather, the distinction between the rain drop and solid precipitation is necessary.

Two years ago, the author noticed that snow flakes left their traces on a photographic paper by the daylight without any photographic operations. Since then he has made it a rule to utilize this phenomenon for the observation of size distribution of precipitation elements. It is the purpose of this paper to show the relation between the size of various precipitation elements and their traces on the photographic paper.

## § 1. Colouring of photographic paper by precipitation.

It is well known that a photographic paper is coloured without development and fixing when it is exposed to the daylight. When precipitation elements fall on the paper and melt on it, the areas wet by them are coloured different from the other unwet areas as shown in photos. 3. By this phenomenon, the traces of rain drops or snow flakes are recorded on the photographic paper.

Generally, the areas wet by precipitation elements are coloured to violet, and the unwet areas to red brown. But for a time, the colours at both areas become violet brown. As the result, the distinction between them soon vanishes. Fortunately, on a sort of photographic paper* in our country, unwet areas are coloured blue, and wet areas red brown, when exposed to

* "Yae FS", "Somei FS", "Yoshino No. 4", "Hinode No. 2", made in Konishiroku Photo. Ind., Ltd.

the direct daylight or a light of relatively short wave length, as shown in Pl. I, Photos. 1~3. In addition to the clear difference between the two colours, these colours are stable if the paper is protected from the direct rays of the sun.

In this work, photographic papers "Hinode No. 2" were mainly used. The direct daylight, brilliant electric lamp of magic lantern, and mercury lamp etc. are suitable for the light source of this purpose. The exposing time ranges from several seconds to ten minutes, according to the intensity of the light used. After the paper was coloured properly, it must be naturally dried and preserved at a place protected from the moisture. As this method needs no photographic operations, it is very suitable for the field work. Even an aged or somewhat fogged photographic paper can be used for this purpose.

## § 2. Observation of rain drop.

It is necessary to calibrate previously the relation between the size of the trace coloured by a rain drop and its diameter.

### a) *Calibration.*

Because the size of the trace by the water drop varies with its falling velocity, the calibration must be made with a water drop of terminal falling velocity. According to Laws report,[1] the height of falling requisite to attain to terminal velocity was selected as in the following table.

Table

| Diameter mm | Height m |
|---|---|
| 0.3~0.6 | 3 |
| 0.8~2 | 6 |
| 3 ~6 | 8.6 |

The drops of diameter 3~6 mm were produced by dropping water from the end of the glass tube as shown in Fig. 1–A. Their diameters were determined by the increase of weight of a photographic paper due to the fall of the drops. Such a large drop leaves a brown trace and a dark brown trace in the brown one as shown in Photo. 1. It is supposed that the drop spreads in the brown area when it falls on the photographic paper, then shrinks to the dark brown area. In this work, the mean diameter of the brown dark area was adopted as the size of the trace. It is difficult to receive the drop of diameter smaller than 3 mm with the paper by the "dropping method," so the spraying method was used as shown in Fig. 1–B. If the water pressure in the nozzle is stable, the distribution of the drop size is invariant. The diameter of those small drops was calculated from the mean weight of many drops of almost equal size which had fallen on the

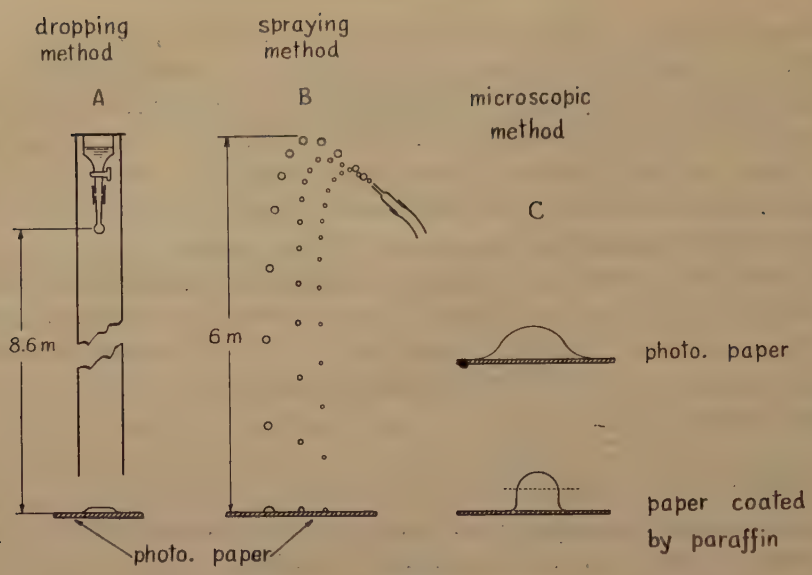


Fig. 1

photographic paper. The trace diameter was measured from the mean of traces on the photographic paper with a magnifying glass. These traces are shown in Pl. II, Photos. 4, 5. The drop size smaller than 0.6 mm was determined by the "microscopic method" in which the side section of the drop which had fallen on a paper was measured with a microscope. For this pupose, a paper coated by paraffine was more suitable than the photographic paper, because the side section of a drop on the photographic paper is too much complicated to calculate the volume from its side section as shown in Fig. 1-C. The size of their traces was observed by the other photographic paper on which other drops are of equal size to that which had fallen on the coated paper. See Photo. 7.

b) *Relation between the size of trace and rain drop.*

Using the apparatuses descrived above, the relation between the trace diameter $D$ (mm) and the water drop diameter $d$ (mm) was acquired, and the result is presented by a full line in Fig. 2. The broken line in the figure is the calibration curve for the "filter paper method" given by Takahashi[2]. The curve coincides approximately with that for the photographic paper method, except the range of diameter smaller than 3 mm. This fact may be explained as follows. The thickness of the water drop shown by the brown area on a photographic paper coincides accidentally with that of filter paper saturated with water, while in small drop range the extension of water by falling on the photographic paper, does not reach to that in the filter paper, because the momentum of falling is small. The size of the brown trace over

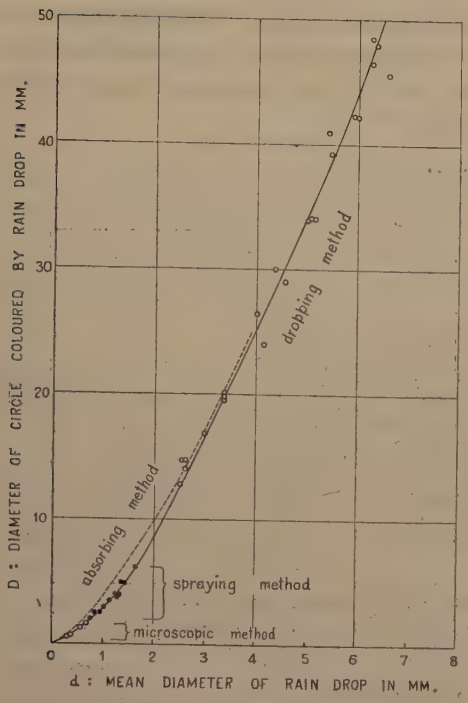


Fig. 2

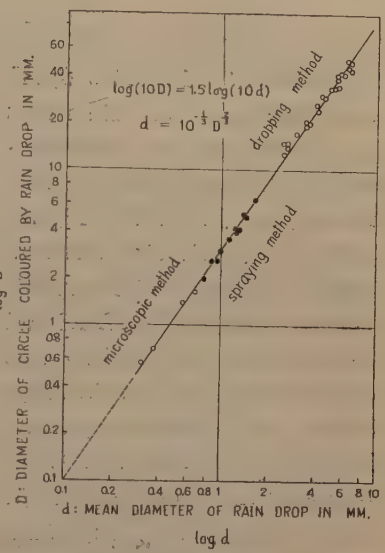


Fig. 3

which a drop has spread by falling is not considered to be related with the sort of the photopaper except in the case of very small drops. The trace sizes on the photographic papers of different sorts were practically equal each other if only smooth photographic papers were used. Considering the stability, the clearness of colour, and from the economical point, photographic papers "Hinode No. 2" (Gaslight) of thin type were suitable for this pupose.

Changing the ordinate of Fig. 2 to logarithmic scale, the result of the calibration is shown by a straight line which passes through the origin as seen in Fig. 3, and is formulated as follows,

$$log\,(10\,D)=1.5\ log\,(10\,d)$$

$$d=10^{-\frac{1}{3}}D^{\frac{2}{3}}=0.46\,D^{\frac{2}{3}}, \qquad (1)$$

where $d$ is the diameter of a rain drop, $D$ mean diameter of a trace by a water drop. This relation corresponds to the relation between the area and the volume. In other words, it is shown that a water drop spreads in a moment at a uniform thickness on a photographic paper. The uniform thickness $h$ (mm) is calculated from the following equation,

$$\frac{\pi}{4}D^2h=volume=\frac{\pi}{6}d^3. \qquad (2)$$

From (1) and (2), $h$ is given by 0.067 mm. The error of the diameter by this method is supposed to be $\pm 4\%$, considering that the difference between the total mass calculated by this method and the one measured by weighing is $\pm 10\%$.

c) *Observation of rain drop distribution.*

Photos. 6, 7 in Plates II, III, show the traces of rain drops on photographic papers obtained at Shiozawa, Niigata Prefecture, in Jan. 1953. Figs. 4 and 5 are each size distributions from the photographic papers. Photo. 7 in Pl. III and Fig. 4 show the narrow size distribution of small rain drops at the end of rain fall process. In Fig. 5, one sees two maximumsof size distribution of medium drop size, as Takahashi[3] pointed out. The capital letter N in these figures shows the number of drops observed.

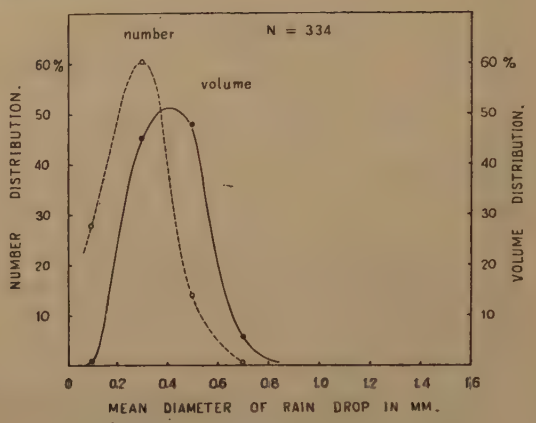


Fig. 4

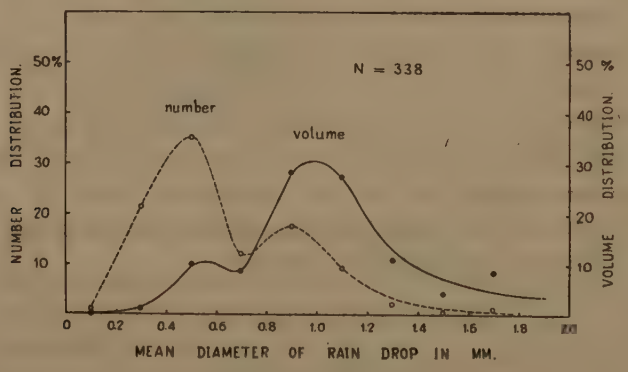


Fig. 5

## § 4. Observation of solid precipitation.

a) *Snow flake or snow crystal.*

It may be considered that a trace by a snow flake corresponds to the horizontal cross-section of the snow flake in falling state, because the ordinary snow flake falls on the photographic paper without spreading, even if it collapses somewhat longitudinarily. Assuming that the snow flake takes a

rotating ellipsoidal form in falling state, the volume of the snow flake is measured as follows,

$$volume = \frac{\pi}{6} ab\sqrt{ab}. \qquad (3)$$

where $a$ is the major axis of the trace, $b$ the minor axis, and $\sqrt{ab}$ is regarded as the diameter of vertical axis of snow flake in falling state. See Fig. 6. $\sqrt{ab}$ is also considered to be the mean diameter of the snow flake,

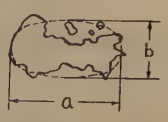


Fig. 6. Trace of a snow flake

$$d=(ab\sqrt{ab})^{\frac{1}{3}}=\sqrt{ab}. \qquad (4)$$

By measuring the increase of the photographic paper by the fall of snow flakes, the mean density of the snow flakes which has fallen on the photographic paper is calculated. The snow crystal was also treated as the small snow flake. The weight of the photographic papers used, was about four grams, and the increase of the weight was of the order of a few hundred milligrams.

In Pl. I, Photo. 3, an example of the traces of the snow flakes obtained at Shiozawa in Jan. 1952 is shown, and the size distribution is shown in Fig. 7.

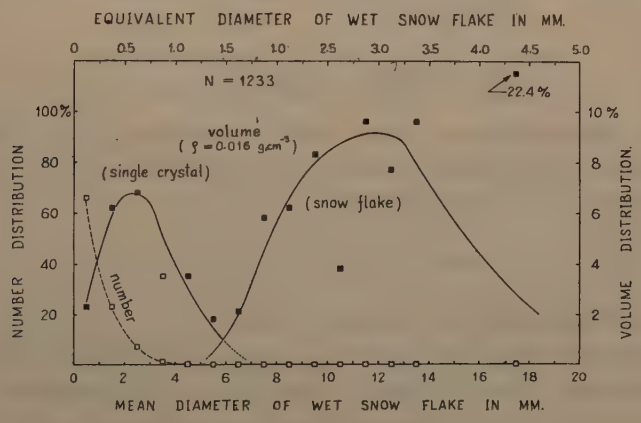


Fig. 7

It is supposed that the larger maximum in the volume distribution shows the distribution of the snow flakes, and the smaller one shows the distribution of the single crystals and the fragments. The followings are the characters of snow flake distribution, that the volume distribution is entirely different from the number distribution comparing the case of rain drop, and that in the range of large diameter, the distribution is very irregular, although the observed snow flakes are numerous enough. For example, the volume distribution 22.4% in the range of diameter 17~18 mm was occupied by only one snow flake. The total volume and the total mass of the snow

flakes on the photographic were 18 $cm^3$ and 280 mg respectively, therefore the mean density was 0.016 g $cm^{-3}$.

In the case of those snow flakes which are scattered when they fall on the photographic paper, it is difficult to determine their volumes. But the mass distribution is obtained by weighing the photographic paper, for the fragments produced from one snow flake are assembled usually to some extent.

b) *Very wet or partially melted snow flake.*

A very wet snow flake spreads horizontally to an uniform thickness when it falls on a photographic paper. But it does not shrink by surface tension like a rain drop, because it contains many ice fragments unmelted. The thickness of the wet snow flake on the photographic paper varies with the grade of its water content in the range from 0.067 mm to about 1 mm. Fortunately the thickness is roughly common to all snow flakes which have fallen at the same time, because their wetness is similar to one another. Measuring their uniform thickness, their volumes and mean diameters are determined as follows,

$$volume = \frac{\pi}{4} D^2 h = \frac{\pi}{6} d^3$$

$$d = \sqrt[3]{1.5h}\, D^{\frac{2}{3}} = 1.15 h^{\frac{1}{3}} D^{\frac{2}{3}}. \tag{5}$$

When the snow flakes are almost melted, therefore, their densities are considered to be about 1 g $cm^{-3}$, their common thickness $h$ is calculated by weighing the total mass on the paper,

$$h = M / \Sigma \frac{\pi}{4} D^2, \tag{6}$$

where $M$ is the total mass of the snow flakes.

Fig. 8 is the result of wet snow flakes obtained at Sapporo in April 1951, when the thickness was uniformly about 1 mm. By comparing the total volume thus calculated with the total mass by weighing, their mean density 0.7 g $cm^{-3}$ was obtained.

c) *Graupel.*

Some time after when a graupel falls on a photographic paper, it is melted into a water drop of hemispherical form, as shown in Fig. 9. In this case, the dark brown area corresponds to the base of the hemisphere. Thus the equivalent diameter of the graupel to the diameter of spherical water drop is obtained as follows,

$$d_w = 2^{-\frac{1}{3}} D' = 0.79\, D', \tag{7}$$

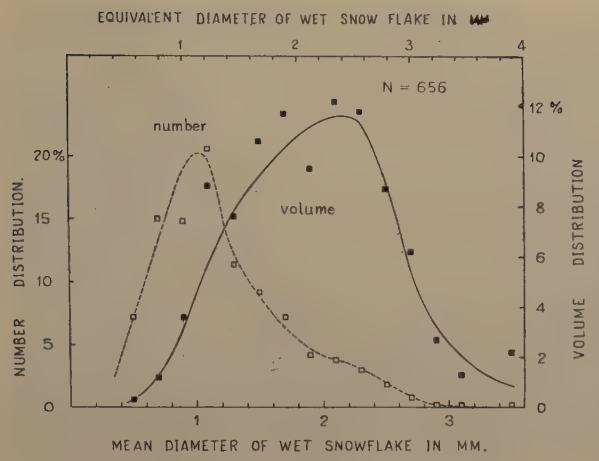


Fig. 8

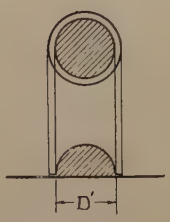


Fig. 9. Trace of graupel

where $d_\omega$ is the equivalent diameter of the graupel, $D'$ the mean diameter of the area of dark brown colour. The volume of a graupel can not be determined by this method. The error in the equivalent diameter of graupel is supposed to be $\pm 3\%$, comparing with the absolute weighing.

An example of the graupel which fell at Yokohama in Jan. 1953 is shown in Photo. 9, and the distribution is presented in Fig. 10. In the figure, one may see that the size distribution of the graupel is similar to that of the rain drop. This suggests that the graupel directly becomes the rain drop when it melts.

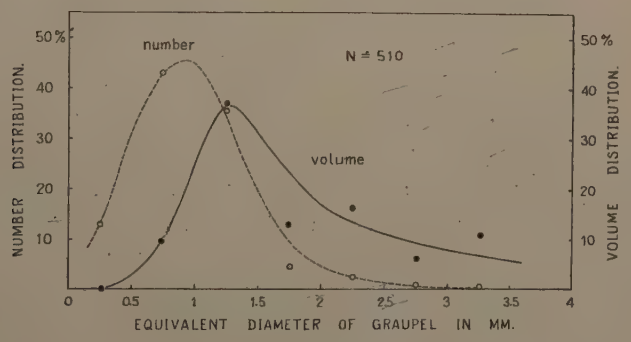


Fig. 10

## § 4. Rain with solid precipitation.

### a) *Rain drop and very wet snow flake.*

When rain drops fall with very wet snow flakes, this photographic paper method is very convenient to distinguish them. As seen in Pl. III, Photo. 8 which was obtained at Shiozawa in Jan. 1953, almost melted snow flakes are easily distinguished from rain drops, for the forms of the traces by the wet

snow flakes are complicated, and some splashes by unmelted ice pieces are seen in the traces. In such a case, the equivalent diameter of almost melted snow flakes is calculated by following considerations. By reducing the sum of the volumes (masses) of rain drops from the total mass of the rain drops and the snow flakes, the sum of the masses of the snowflakes is obtained. Using (5) and (6), the thickness and the equivalent diameter are calculated.

The size distribution shown in Fig. 11 was thus obtained. In the figure,

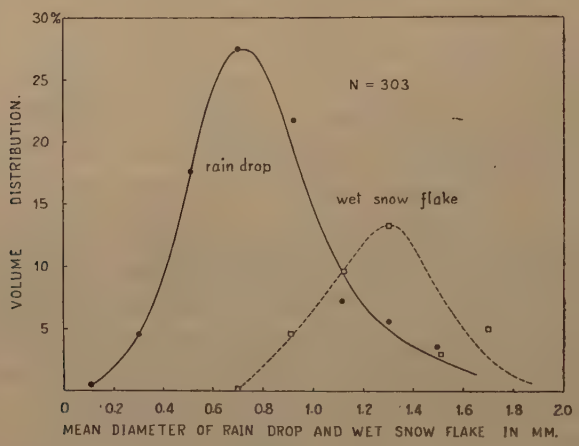


Fig. 11

one sees that the size distribution of very wet snow flakes deviates to the larger range, in other words, small snow particles, such as single snow crystals or fragments had melted earlier than the snow flakes. This is a type of the sleety weather.

b) *Rain and wet graupel.*

In Dec. 10, 1952, many ice particles were observed on a photographic paper at Yokohama, being mixed with rain drops, though these ice particles were not noticed until they had fallen on the photographic paper. The particles remained for some time unmelted, and the traces were coloured more powerfully than that of rain drops. In order to make sure, the arrows were marked to their traces as shown in Photo. 10. The author thinks that the particles were wet graupels, for they were not transparent. And if the particles originate from refrozen rain drops, that is, sleets they must be smaller than the rain drops. For the freeze must begin from the smaller rain drops. But their volumes (calculated from semispherical form) were rather larger than that of rain drops.

In Fig. 12, the size distribution of the rain drops and graupels which were obtained from Pl. IV, Photo. 10, are shown. Each diameter was calculated by

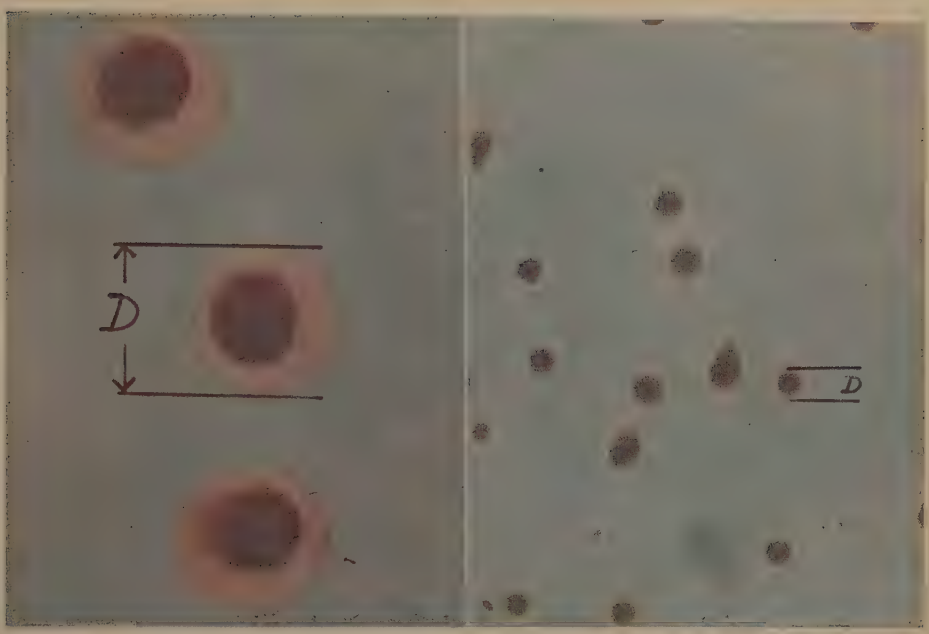


Photo. 1 : ×1
Water drops of diameter
3.4 mm.

Photo. 2 : ×1
Water drops of diameter
1.3 mm.

Photo. 3 (fig. 7) : ×1
Snow flakes and snow crystals.
A part of Cabinet size, expos. time : 30 sec., 10h50m Jan. 31, 1952, at Shiozawa.

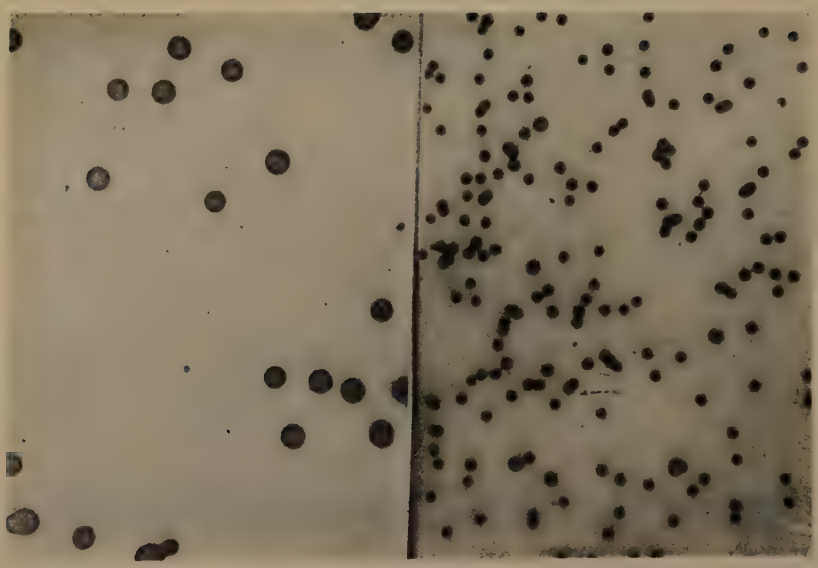

Photo. 4: ×1
Water drops of diameter 1.0 mm.

Photo. 5: ×1
Water drops of diameter 0.56 mm.

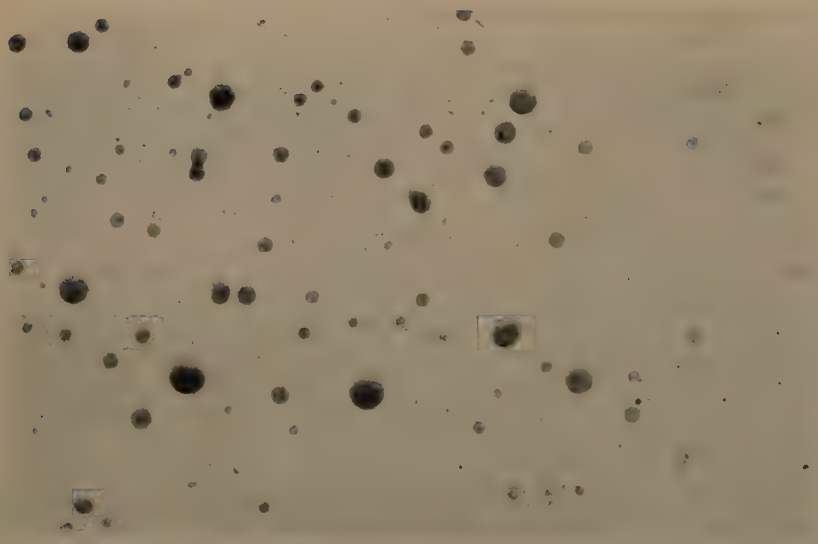

Photo. 6 (fig. 5): ×1
Rain drops.
A part of Cabinet size, expos. time: 7 sec.
$12^h42^m$, Jan. 25, 1953, at Shiozawa.

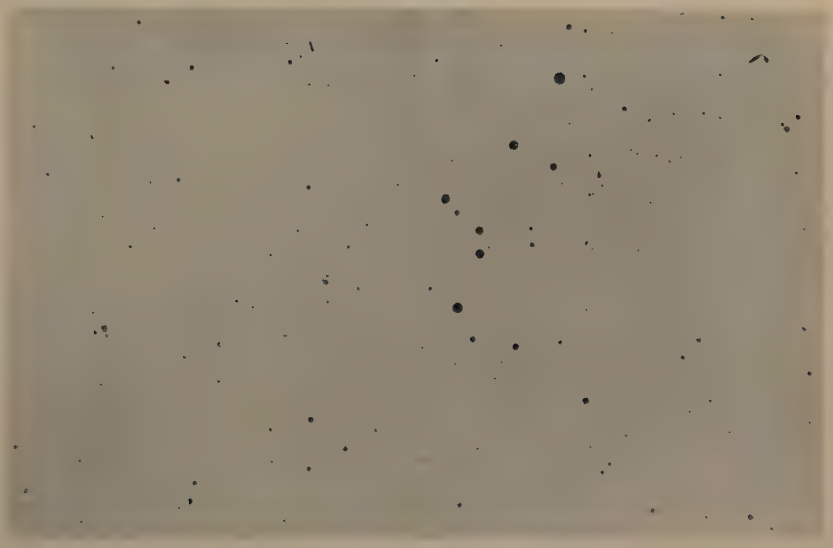

Photo. 7 (Fig. 4): ×1
Rain drops.
A part of Cabinet size, expos. time: 2 min.
13h20m, Jan. 25, 1953, at Shiozawa.

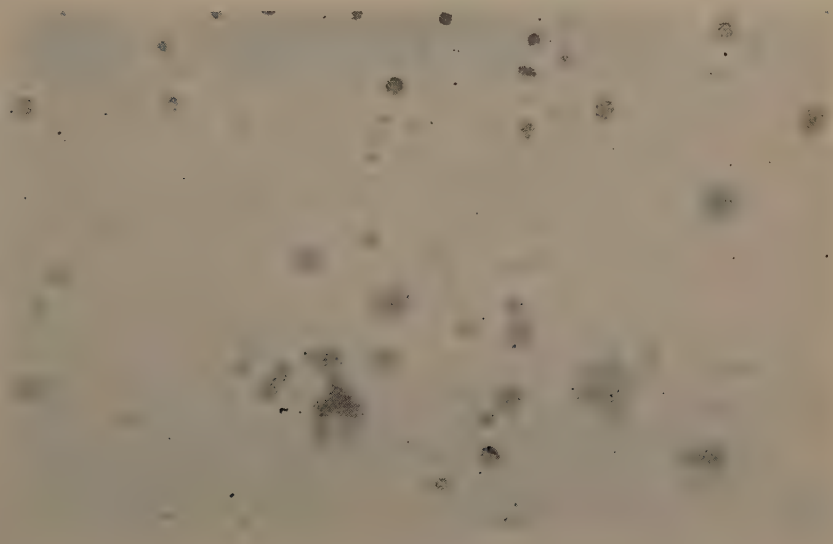

Photo. 8 (fig. 11): ×1
Rain drops and wet snow flakes.
A part of Cabinet size, expos. time: 10 sec.,
13h10m Jan. 25, 1953, at Shiozawa.

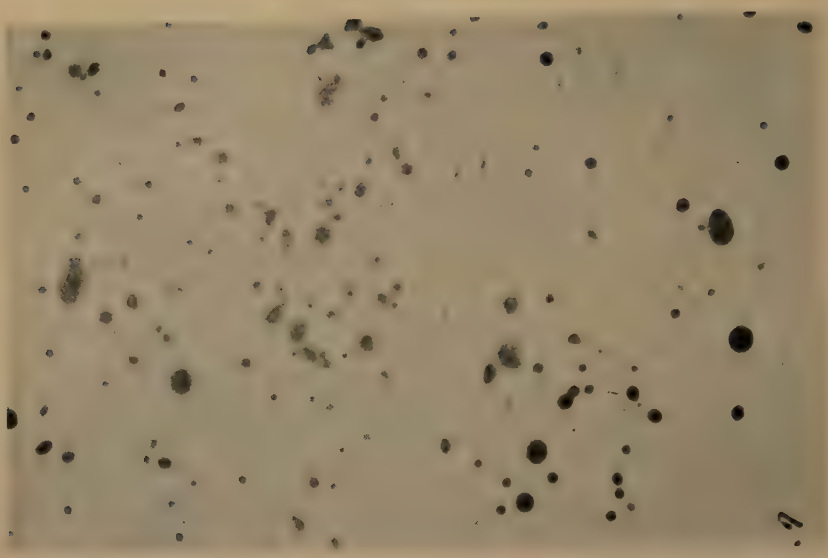

Photo. 9 (Fig. 10): ×1
Graupels.
A part of Cabinet size, expos. time: 30 sec.
23h15m Jan. 7, 1953, at Yokohama.

Photo. 10. (Fig. 12): ×1
Rain drops and wet graupels, graupels being marked by arrows.
A part of Cabinet size, expos. time: 30 sec.
12h30m Dec. 10, 1952, at Yokohama.

each calibration method. In this case also, the graupels distribute in the range of diameters larger than those of rain drops.

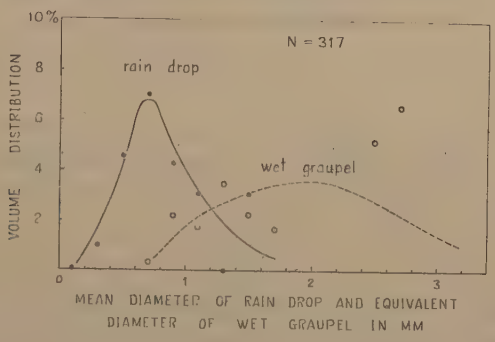


Fig. 12

## Conclusion

A simple method by the photographic paper which is applicable to all precipitation elements, was proposed. But the method has yet following faults. In a heavy precipitation, the traces of large rain drops mix mutually. The volumes of those snow flakes which scatter on the photographic paper can not be measured. These faults are common to all other methods in which the precipitation elements are received by a paper, but they shall be removed in the near future. In a rather temperate climate, the author thinks, this photographic method is most convenient.

Recently the author has known that Dr. Smith had used already a sensitive paper for the approximate measurement of the rain drop size on an aircraft, but his detailed procedures have not been reported yet.

In conclusion, the author wishes to express his best thank to Misters. B. Arai, T. Watanabe and M. Matsumoto for their collaborations of this work. The author is also indebted to Mr. M. Shōda who gave him the facilities for the observation in this work.

## References

1) Laws, J. O., 1941: Measurement of the fall-velocity of water drops and rain drops, Trans. Amer. Geophys. Union, p. 709.
2) Takahashi, Y., 1934: Measurement of rain drop size (in Japanese): Tenki to Kikō, Vol. 1, No. 2, p. 63.
3) Takahashi, Y., 1935: Über Regen und Regentropfen, J. Met. Soc. Japan, Ser. 2, Vol. 13, p. 67.
4) Smith, E. J., 1950: Observations of rain from non-freezing clouds, Quart. J. R. Met. Soc., Vol. 76, p. 33.

[Science Reports of the Yokohama National University, Sec. I, No. 3, 1954]

# Low Frequency Divergence in Quantum Field Theory

By

**Daisuke ITŌ and Hiroshi TANAKA**

(Received November 3, 1953)*)

**Abstract**

The well known divergences due to the energy conservations in the intermediate states are considered, from the point of view of the graphical structure and of the field reactions.

## § 1. Introduction

In contrast to the ultraviolet divergence, the low frequency divergences due to the coincidence of poles in transition matrices or in transition probalities in the quantum field theory are generally regarded as a defect of the perturbation theory. These difficulties should disappear in principle. However, they stand sometimes in the way of computational works with the Feynman-Dyson's covariant S-matrix formalism, especially in the process involving mesons. Therefore, the special discussion of these divergences is also a matter of practical importance.

In quantum electrodynamics, the low frequence divergences are conveniently classified into three cathegories; the first of them appears from the single pole of matrix elements corresponding to the energy conservation in the intermediate states. As is well known, the divergences of this type are of quite formal nature and they raise no difficulties, as they are removed by well known procedure of the amplitude-renormalization of the wave functions, or by other suitable limiting processes, such as the principal value evaluation, etc. Therefore, they are out of our consideration. The second type divergence originates from the matrix element which is finite certainly but not uniformly. A typical example of this divergence is so called "*infra-red catastroph*", that is, the matrix elements of bremsstrahlung are certaintly finite, but their total transition probability diverges at the low frequency limit. The divergence of the third kind comes from the coincidence of poles in a transition matrix. As is well known, the coincidence of the displaced poles corresponds to the excitation of the real process or to other competing processes. Therefore, the divergence of this type is regarded as a "*resonance*

*) The content of the present work was published in Japanese more one or two years ago, separated to several papers. So, we summarize here our main considerations.

*catastrophe*" and they will disappear whenever the effects of field reactions, i. g., the effect of radiation damping, etc., are properly taken into account.

In the meson theory, it is evident that no infra-red catastrophe can appear on account of the non-vanishing meson mass. The reason why this is so is readily seen if we note the fact that the infra-red catastrophe originates from the vanishing energy denominators in the perturbation theory. As a simplest example we consider the process of bremsstrahlung in Fig. 1. As the real emission of a quantum $k$ on the transition from free particle state $p$ into a free state $p-k$ is prohibited by the conservation law, the matrix element of this process is certainly finite, except only for one case $k=0$, where the energy denominator of the intermediate propagator vanishes. The element is finite in almost everywhere, however, it is not uniform. But in the corresponding meson process, $k=0$ is excluded by non-vanishing meson mass. This is the reason why no infra-red catastrophe appears in the emission process of meson.

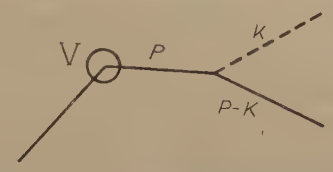

Fig. 1. $V$: external field of force

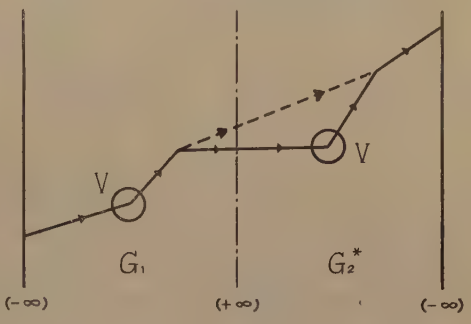

Fig. 2

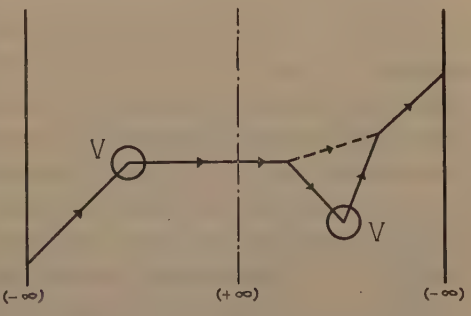

Fig. 3

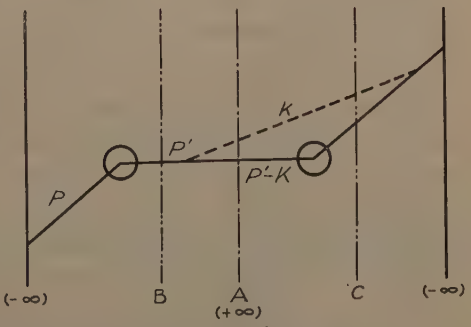

Fig. 4

But in the case of the corresponding process of meson-decay where the meson $p$ in intermediate state decays into two lighter particles, a free particle state is allowed as the intermediate state. Therefore, new divergence corresponding to "*infra-red catastrophe*" re- appears in this decay-process. Let us now consider this "*infra-red-like catastrophe*" divergence. For this purpose, it is convenient to introduce a Feynman-diagram of transition probability. This diagram is constructed from two ordinary Feynman-diagrams $G_1$ and

$G_2$, as follows. We define here the conjugate diagram $G^*$ of $G$, which is obtained by reversals of all direction of the propagating particles in $G$. Put $G_2^*$ at the right edge of $G_1$ and join each lines smoothly as illustrated in Fig. 2, then we obtain the Feynman-diagram of the transition probabilities constructed from $G_1$ and $G_2$. In the same way, we have Fig. 3 as a Feynman-diagram of a radiative correction term for the transition probability of the elastic scattering by an external field of force. Here it is notable that Fig. 2 has the same structure as that of Fig. 3 with different position of the "*line of observation*" $(+\infty)$. A part of the transition probability, which results from a cross term of the matrix elements $H_1$ and $H_2$ corresponding to the graphs $G_1$ and $G_2$ respectively,

$$W=\frac{2\pi}{h}<H_1 H_2> \qquad (1)$$

is readily obtained from these diagrams according to the usual rules of Feynman, provided that the "*internal*" lines which cross the line $(+\infty)$ in Fig. 2 must be regarded as the out-going free waves in the final state, that is to say, the observation- (or projection-) operators to the final states are hidden on this line.

The problem of the infra-red catastrophe has been discussed by many authors,[1] and clarified that the infra-red divergence appeared in the brems-strahlung is cancelled out by that of the radiative correction of the elastic scattering process. Recently, T. Kinoshita[2] analyzed this problem in more detail and demonstrated that cancellations are accomplished term by term between the parts of transition probabilities that have the Feynman-diagram of same structure. Extending his result, it is shown that the same procedure can be successfully applied to the case of the *infra-red-like catastrophe* divergence in the meson-decay process and finite rate of decrease of initial state probality is obtained in each order approximation of perturbation. This method gives, however, no finite results for each one of the component process. This situation often limits the practical applicability of this method, inspite of its theoretical interest. In order to obtain the finite result for each component process, we have to take into account the effects of the field reactions, such as the effects of radiation damping. The effect of radiation damping is introduced here entirely within the frame-work of Feynman-Dyson's covariant theory of S-matrix. A covariant generalizatien of Heitler's theory of radiation damping has been proposed by T. Miyajima and N. Fukuda.[3] So far as the effect of radiation damping is concerned, our

1) F. Bloch and A. Nordsieck, Phys. Rev. 52 (1937), 1045 (L)
W. Pauli and M. Fierz, Nuovo Cimento 15 (1938), 167.
W. Braunbek and E. Weinmann, Z. S. f. phys. 110 (1938), 360.
2) T. Kinoshita, Prog. Theor. Phys. 5 (1950), 1045 (L).
3) N. Fukuda and T. Miyajima, Prog. Theor. Phys. 5 (1950), 849.

method gives, of course, equivalent results with that of Miyajima and Fukuda. The difference consists in the way of taking into account the virtual processes. As our method is developed completely in conformity with the Dyson's S-matrix theory[4], it is convenient for the renormalization, for S-matrix theoretical characterization and for application to the practical problems.

## § 2. Infra-red-like catastrophe aspects.[5),6)]

In this section, let us show that the *infra-red-like catastrophe* divergence which appeared in the meson-decay process is removed by the same procedure as used in the theory of *infra-red catastrophe*. In order to clarify the correspondence to the ordinary infra-red catastrophe, we consider the meson-analogue of bremsstrahlung, i.e. the process in which a heavy meson (mass $M$) decays into two lighter mesons (mass $m$ and $m'$) in the course of deflection by an external field of force $V$. (See Fig. 1) In contrast to the ultra-violet divergence, the type of the relevant particles is of minor importance. Therefore, we may choose the simplest model for each particle without any loss of generality. As an illustrating example, let us consider a part of the transition probability, the Feynman diagram which is illustrated in Fig. 4. Using following the simplest model;

$$\begin{aligned} &U(x) && : \text{ charged heavy scalar field of mass } M \\ &\psi(x) && : \text{ charged light scalar field of mass } m \\ &\phi(x) && : \text{ neutral scalar field of mass } m' \\ &V(x) && : \text{ external field} \end{aligned} \tag{2.1}$$

and their mutual interactions;

$$H(x) = g(\bar{U}\psi + \bar{\psi}U)\phi \tag{2.2}$$

$$K(x) = \bar{U}\,U\,V \tag{2.3}$$

$$K'(x) = \bar{\psi}\,\psi\,V \tag{2.4}$$

the transition probability $W_A$ of the decay process "A"[**)] is calculated as

$$W_A = \frac{g^2}{4(2\pi)^8}\,\frac{1}{E_p}\int_{\epsilon_k=\mu^2}^{\epsilon_{max}}\frac{dK}{\epsilon_k}\int\frac{dP'}{e_{p'-k}}\,\frac{|V(P-P')|^2}{[E_p^2-E_{p'}^2][e_{p'-k}-e_{p-k}]}\times$$
$$\times\,\delta(E_p-e_{p'-k}-\epsilon_k) \tag{25}$$

where $(E_p, e_p, \epsilon_p)\equiv\sqrt{P^2+(M^2, m^2, \mu^2)}$ respectively. The integand has two poles. As is easily seen, one of them corresponds to the energy conservation

4) F. J. Dyson, Phys. Rev. 75 (1949), 1736.
5) D. Ito, Prog. Theor. Phys. 6 (1951), 1020 (L) and 1022 (L).
6) J. Edden, Proc. Roy. Soc. 210 (1952), 388.
**) The process "A" in Fig. 4 is the same with Fig. 2.

in the intermediate state B, in Fig. 4, and the other corresponds to the energy conservation in the intermediate state C. In the vicinity of these poles, $W_A$ diverges logarithmically and takes the following asymptotic forms.

$$W_A(B)=\frac{g^2}{4(2\pi)^8}\frac{1}{E_p}\int\frac{dK\,dP'}{2E_{p'}\,e_{p'-k}\epsilon_k}\frac{|V(P-P')|^2}{e^2_{p'-k}-e^2_{p-k}}\frac{\delta(E_p-e_{p'-k}-\epsilon_k)}{e_{p'-k}+\epsilon_k-E_{p'}} \tag{2.6}$$

in this case $(\epsilon_k\sim E_{p'}-e_{p'-k})$,

$$W_A(C)=\frac{g^2}{4(2\pi)^8}\frac{1}{E_p}\int\frac{dK\,dP'}{2e_{p-k}\,e_{p'-k}\epsilon_k}\frac{|V(P-P')|^2}{E^2_p-E^2_{p'}}\frac{\delta(E_p-e_{p-k}-\epsilon_k)}{e_{p'-k}-e_{p-k}} \tag{2.7}$$

in this case $(e_{p'-k}\fallingdotseq e_{p-k})$

In analogy with the theory of ordinary infra-red catastrophe, let us examine the transition probability $W_B$ of the elastic scattering process "B" in Fig. 4.[**)] In this case, we have to assume the line B as the line of the observation. $W_B$ is calculated as follows;

$$W_B=\frac{g^2}{4(2\pi)^8}\frac{1}{E_p}\int_{\varepsilon_k=\mu}^{\infty}\frac{dK}{\epsilon_k}\int\frac{dP'}{E_{p'}}\frac{|V(P-P')|^2}{[e^2_{p-k}-(E_p-\epsilon_k)^2][e^2_{p'-k}-(E_{p'}-\epsilon_k)^2]}\times$$
$$\times\delta(E_p-E_{p'}) \tag{2.8}$$

Two poles of the integrand correspond to the conservation of energy in the intermediate states A and B respectively, and the asymptotic forms at these points are

$$W_B(A)=\frac{g^2}{4(2\pi)^8}\frac{1}{E_p}\int\frac{dK\,dP'}{2E_{p'}\,e_{p'-k}\epsilon_k}\frac{|V(P-P')|^2}{e^2_{p-k}-e^2_{p'-k}}\frac{\delta(E_p-E_{p'})}{e_{p'-k}+\epsilon_k-E_p} \tag{2.9}$$

in this case $(\epsilon_k\fallingdotseq E_p-e_{p'-k})$

$$W_B(C)=\frac{g^2}{4(2\pi)^8}\frac{1}{E_p}\int\frac{dK\,dP'}{2E_{p'}\,e_{p-k}\epsilon_k}\frac{|V(P-P')|^2}{e^2_{p'-k}-e^2_{p-k}}\frac{\delta(E_p-E_{p'})}{e_{p-k}+\epsilon_k-E_p} \tag{2.10}$$

in this case $(\epsilon_k\fallingdotseq E_p-e_{p-k})$

Further, we have to take into acount another process whose Feynman-diagram is obtained from Fig. 4, assuming the line C as the observation line. This is a process of meson-decay accompanied by the double scattering by the external field, which has no analogue in the corresponding photon process. The transition probability $W_C$ of this process "C" turns out to be

$$W_C=\frac{g^2}{4(2\pi)^8}\frac{1}{E_p}\int_{\varepsilon_k=\mu}^{\varepsilon_{max}}\frac{dK}{\epsilon_k}\int\frac{dP}{e_{p-k}}\frac{|V(P-P')|^2}{[E^2_{p'}-E^2_p][e^2_{p'-k}-e^2_{p-k}]}\times$$
$$\times\delta(E_p-e_{p-k}-\epsilon_k) \tag{2.11}$$

and the asymptotic forms at A and B are

[**)] The process "B" in Fig. 4 is the same with Fig. 3..

$$W_C(A)=\frac{g^2}{4(2\pi)^8}\frac{1}{E_p}\int\frac{dK\,dP'}{2e_{p-k}e_{p'-k}\epsilon_k}\frac{|V(P-P')|^2}{E_{p'}^2-E_p^2}\frac{\delta(E_p-e_{p-k}-\epsilon_k)}{e_{p'-k}-e_{p-k}}$$

in this case $(e_{p'-k}\fallingdotseq e_{p-k})$ (2.12)

$$W_c(B)=\frac{g^2}{4(2\pi)^8}\frac{1}{E_p}\int\frac{dK\,dP'}{2E_{p'}e_{p-k}\epsilon_k}\frac{|V(P-P')|^2}{e_{p'-k}^2-e_{p-k}^2}\frac{\delta(E_p-e_{p-k}-\epsilon_k)}{E_{p'}-e_{p-k}-\epsilon_k} \quad (2.13)$$

in this case $(\epsilon_k\fallingdotseq E_{p'}-e_{p-k})$

Comparing these asymptotic forms of divergent integrals, we can readily find out a kind of "reciprocity relation" holding between them,

$$\begin{aligned}&W_A(B)=-W_B(A)\\&W_B(C)=-W_C(B)\\&W_C(A)=-W_A(C)\end{aligned} \quad (2.14)$$

From the view-point of the asymptotic forms of the divergences, we may summarize the above results as follows

$$\begin{aligned}&W_A\sim\quad\quad W_A(B)+W_A(C)\\&W_B\sim W_B(A)\quad\quad+W_B(C)\\&W_C\sim W_C(A)+W_C(B)\end{aligned} \quad (2.15)$$

On account of these asymptotic forms and the above reciprocity relations, the infra-red-like catastrophe divergences are cancelled out from the total rate of decrease of the initial state-probability.

In this way, the divergence appeared in the process of our meson-decay is cancelled out by simultaneous consideration of the processes of the elastic scattering and of the decay with double scattering. This is nothing but the way, by which the ordinary infra-red catastrophe has been removed. Therefore, the divergences due to the energy conservation in intermediate states of the meson process are of the same nature as that of the "infra-red catastrophe" and they are removed by natural generalization of the method used in the case of quantum electrodynamics.

Moreover, the above consideration reveals us that the reason why the cancellations of the infra-red-like divergences are possible, consists in the validity of the reciprocity relations. Of course, these relations also have played essential roles in the case of the ordinary infra-red catastrophe, but we could not notice them on account of the over-simplifications of the mechanism due to the simpler nature of photons. Accordingly, our method will be extended to more general cases, if we are able to give a general proof of the validity of the reciprocity relations. In order to give it, let us consider a Feynman-diagram of the transition probability of more general form, as illustrated in Fig. 5, where each one of $G_1$, $G_2$ and $G$ represents arbitrary

graph. Referring to this graph, the reciprocity relation to be proved is formulated as follows; The asymptotic form of divergence $W_A(B)$ due to the energy conservation in intermediate state B of the process "A" has just the same form and opposite sign as the asymptotic form $W_B(A)$ of similar divergence due to the conservation in A of the process "B". Assuming again all relevant particles are scalar, we obtain the following asymptotic forms after some elementary calculations

$$W_A(B)=\prod_{i=1}^{n}\int\frac{dP_i}{E_i(P_i)}\prod_{j=1}^{n}\int\frac{dq_j}{e_j(q_j)}\,\frac{f(P_1,E_1(P_1)\cdots;q_1,e_1(q_1)\cdots;)}{\sum e_j(q_j)-\sum E_i(P_i)}\times$$

$$\times\delta(E_{initial}-\sum_{j=1}^{n}e_j(q_j)) \tag{2.16}$$

in this case $(\sum e_j \fallingdotseq \sum E_i)$

$$W_B(A)=\sum_{i=1}^{n}\int\frac{dP_i}{E_i(P_i)}\prod_{j=1}^{n}\int\frac{dq_j}{e_j(q_j)}\,\frac{f(P_1,E_1(P_1);\cdots;q_1,e_1(q_1)\cdots;)}{\sum E_i(P_i)-\sum e_j(q_j)}\times$$

$$\times\delta(E_{initial}-\sum_{i=1}^{n}E_i(P_i)) \tag{2.17}$$

in this case $(\sum E \fallingdotseq \sum e)$

These results show that the reciprocity relation

$$W_A(B)=-W_B(A) \tag{2.18}$$

holds for the most general cases. The possibility of the cancellation of the divergences due to the energy conservations in intermediate states by means of simultaneous consideration of related processes is an immediate consequence of this reciprocity relation. Accordingly, the method once applied to the cancellation of the infra-red catastrophe is now able to be extended to more general cases of such low frequency divergences as arising in the meson theory.

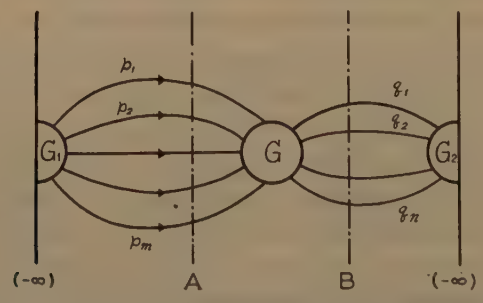


Fig. 5. $E_i(P_i)\equiv\sqrt{P_i^2+M^2}$ $e_j(q_j)\equiv\sqrt{q_j^2+m_j^2}$

## §3. Consideration of field reaction

In the previous section, it is clarified that the method used in the theory of infra-red catastrophe can also be applied to cancellations of the low frequency divergences appearing in the meson-decay processes. However,

we could have only a finite rate of decrease of the initial state-amplitude. The transition probability of each component process which transfers the system in its initial state into each final state is still divergent, therefore, we could have no information about these component processes. This situation limits considerably the applicability of this method, inspite of their theoretical interest. In order to obtain a finite result for each component process, the effects of field reactions must be taken into account.

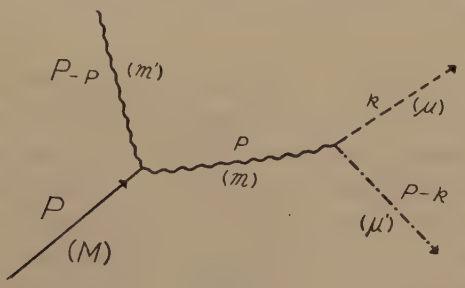


Fig. 6

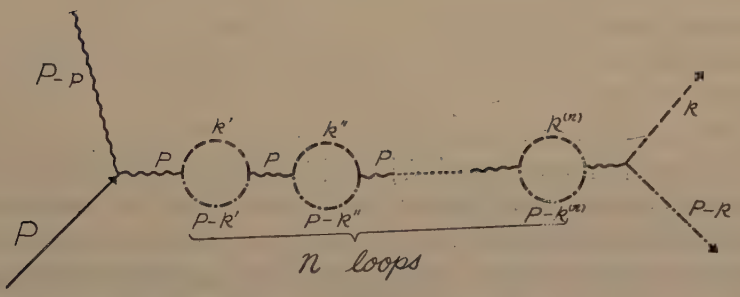


Fig. 7

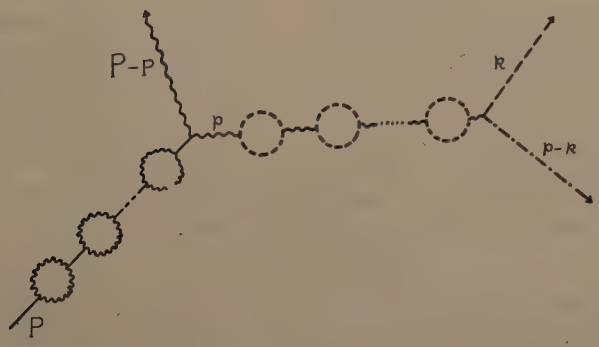


Fig. 8

(1) *general survey*

Let us begin with a simple example; the double decay process of mesons, in which a heavy meson (mass $M$) decays into two lighter mesons (masses

$m$ and $m'$) and then one of them (*say*, mass $m$,) decays into two lighter mesons (mass $\mu$ and $\mu'$). The Feynman graph of this process is illustrated in Fig. 6. According to the perturbation theory, the lowest order approximation of the total transition probability diverges at the point which corresponds to the free particle state of the intermediate particle $m$. As mensioned above, the divergence of this type is of the same nature as that of the infra-red catastrophe in quantum electrodynamics and will be removed by the same method.

Apart from the divergence-problem, however, the description by the lowest order approximation of perturbation is expected to be qualitatively very incomplete. Because, unstable mesons are fated to decay sooner or later, and they will certainly decay into lighter mesons in a very long lapse of time. And whenever the rate of decay of the intermediate meson $m$ is greater than that of the creation, the rate of the total process will be determined by the decay probability of the mother meson $M$ alone, that is, the S-matrix element of the total process $M \to m + m' \to m' + \mu + \mu'$ will be in the limiting case independent of the detailed forms of the interaction operator describing the latter process $m \to \mu + \mu'$. It is probably impossible to describe such situations by the lowest order approximation of perturbation alone. The above situation is clearly a result of very long duration of time after the creation of meson $m$ in comparison with their life. The transition probability $W \sim |<\mu\mu'|H_2|m><mm'|H_1|M>|^2 t$ calculated to the lowest order approximation has its meaning only if the duration of time is very small in comparison with the life time. Nevertheless, if we tend $t$ to infinity in order to know about the situation in infinite future, $W$ increases beyond all limits.[7] This is nothing but the space-time interpretation of the infra-red-like catastrophe divergence, as the linear time dependence is a result of the energy conservation in the intermediate states. Therefore, the divergence will disappear in such theory as is able to describe correctly the behavior of transition probability of the total process.

From above considerations, it seems natural to remove the divergence by considering the effect of damping in the intermediate states. In view of the characteristic features of damping, it is expected that the situation will probably be described by the following natural interpolation, at least as an approximation.

$$\left.\begin{array}{ll} W \sim |<mm'|H_1|M>|^2 & (t \gg life) \\ W \sim |<\mu\mu'|H_2|m><mm'|H_1|M>|^2 t & (t \ll life) \end{array}\right\} \to W \sim |<M|H_1|mm'>|^2 \times$$

$$\times (1 - e^{-|<m|H_2|\mu\mu'>|^2 t}) \qquad (3.1)$$

This is not an unfounded expectation. When the proper frequency of the

7) B. A. Lippmann and J. Schwinger, Phys. Rev. 79 (1950), 469.

meson is larger than the uncertainty of energy due to the finite life time $\frac{2}{\gamma}$, that is, when the particles in intermediate state can be regarded as if it were in its free particle- state, the whole process may be a series of the natural radioactivity. In the series A, B, C, of natural radioactivity, the probabilities of finding the atomic nuclei A, B, C, respectively, $n_A$, $n_B$ and $n_C$ are solutions of the following equation

$$\dot{n}_A=-\Gamma n_A, \quad \dot{n}_B=-\gamma n_B+\Gamma n_A, \quad \dot{n}_C=+\gamma n_B$$

with initial condition

$$n_A(0)=1, \quad n_B(0)=n_C(0)=0$$

where $\Gamma$, and $\gamma$ represent the transition probabilities of the process $A\to B$, and $B\to C$, respectively. The rate of the total process $W=\dot{n}_C$ is calculated as

$$W=\Gamma(1-e^{-\gamma t}) \tag{3.2}$$

This is just the same form as (3.1). Therefore, the correct theory has to have a solution which reduces to (3.1) when the intermediate state could be regarded as a state of free particle. Such solution is really obtained if we take into account the radiation damping in intermediate state in accordance with the theory of Weisskopf and Wigner.[8)]

(2) *damping effect in intermediate state*

Suggested by the above rough consideration, let us consider the corrections of the internal line by succession of the self-energy loops consisting of the pair of lighter mesons $\mu$ and $\mu'$, as illustrated in Fig. 7. Assuming all the particles are scalar and, their interactions are

$$H_1=g_1\psi^*\phi\,\phi'+conj. \qquad H_2=g_2\phi^*\,a\,a'+conj. \tag{3.3}$$

where $\psi, \phi, \phi', a$, and $a'$ are fields of meson $M, m, m', \mu$ and $\mu'$ respectively. We obtain the following expression as total contribution to S-matrix from all graphs having the forms given in Fig. 7.

$$S=\frac{ig_1g_2}{(2\pi)_3}\sqrt{\frac{1}{16E_p(E_p-\epsilon_k-\epsilon'_{p-k})\epsilon_k\epsilon'_{p-k}}}\,\frac{1}{P^2+m^2-i(\epsilon+\Gamma(p))} \tag{3.4}$$

where
$$\Gamma(p)\equiv\frac{g_2^2}{(2\pi)_4}\int\frac{(dk'')}{[k''^2+\mu^2-i\epsilon][(p-k'')^2+\mu'^2-i\epsilon]} \tag{3.5}$$

represents the self energy operator of the internal line with propagation vector $p$. The transition probability $W$ is calculated from above S-matrix as

$$W=\frac{(g_1g_2)^2}{(2\pi)^5}\int\frac{dP\,dK}{16E_p(E_p-\epsilon_k-\epsilon'_{p-k})\,\epsilon_k\epsilon'_{p-k}}\,\frac{1}{|P^2+m^2-i(\epsilon+\Gamma(p))|^2} \tag{3.6}$$

8) V. Weisskopf and E. Wigner, Z. S. f. Phys. 63 (1930), 54 and 65 (1930), 18.

In the decay process, $\Gamma(p)$ is, in general, complex and given by

$$-i\Gamma(p) \equiv \delta m^2(p) + ip_0 \frac{\gamma(p)}{2} \tag{3.7}$$

$$= \frac{g_2^2}{(2\pi)^4} \int (dk'') \left[ \pi \left( \frac{\delta((p-k'')^2+\mu'^2)}{k''^2+\mu^2} + \frac{\delta(k''^2+\mu^2)}{(p-k'')^2+\mu'^2} \right) + \right.$$

$$\left. + i\pi^2 \delta((p-k'')^2+\mu'^2)\, \delta(k''^2+\mu^2) \right] \tag{3.8}$$

where the real part $\delta m^2(p)$ represents the self-energy of the intermediate particle containing a correction of mass, an effect of level-shift etc., and was a principal matter of concern in the theory of the renormalization. The imaginary part $ip_0 \frac{\gamma(p)}{2}$ contains in this case a non-vanishing part

$$\gamma(p) = 2\pi g_2^2 \int \frac{dK/(2\pi)^3}{8p_0 \epsilon_{k''}(p_0-\epsilon_{k''})}\, \delta(p_0-\epsilon_{k''}-\epsilon_{p-k''}) \tag{3.9}$$

As is readily seen this is nothing but the total transition probability of the second decay process $m \to \mu + \mu'$. Putting $e_p \equiv \sqrt{P+(m^2+\delta m^2(p))}$ we have

$$W = \frac{(g_1 g_2)^2}{(2\pi)^5} \int \frac{dP\, dp_0\, dK}{16 E_p (E_p - p_0) \epsilon_k \epsilon'_{p-k}} \frac{\delta(\epsilon_k + \epsilon'_{p-k} - p_0)}{(e_p^2 - p_0^2)^2 + (p_0\gamma(p)/2)^2} \tag{3.10}$$

As $\gamma(p)$ does not vanish, we obtain always convergent $W$. The functional forms of $\delta m^2(p)$ and $\gamma(p)$ are usually very complicated and it is not a simple matter to evaluate the integral rigoroutly. It is not our present purpose to calculate the transition probability exactly, but to verify the fact that the result is divergence-free and is insensitive to the detailed nature of the interaction describing the second decay process, whenever the free particle state is dominant in the intermediate state and the latter decay is much faster than the first. Therefore, we calculate it here approximately in the case of "sharp resonance" where $\gamma(p)$ is small enough to replace the argument $p$ of $\delta m(p)$ and $\gamma(p)$ by its resonance value. Then, the evaluation of the integral is elementary and reduces to

$$W = 2\pi g_1^2 \int \frac{(dP)/(2\pi)^3}{8E_p(E_p-e_p)e_p}\; 2\pi g_2^2 \int \frac{dK/(2\pi)^3}{8e_p \epsilon_k (e_p - \epsilon_k)} \times$$

$$\times \delta(e_p - \epsilon_k - \epsilon'_{p-k}) \Big/ \frac{\gamma(p)}{2} \tag{3.11}$$

On account of the definition of $\gamma(p)$, this reduces further to

$$W = 2\pi g_1^2 \int \frac{(dP)/(2\pi)^3}{8E_p\, e_p (E_p - e_p)} \tag{3.12}$$

This is nothing but the transition probability of the decay process of the first step $M \to m + m'$. Thus, under the condition described above, the transi-

tion probability of the total process is determined by the first decay process alone, and does not depend upon the detailed natures of the second decay as expected before.

(3) *time- dependence of transition probability*

The above results are based upon the S-matrix theory and are able to predict only the situation in infinite future. The next task is to examine the time dependence of the transition probability.

The transformation function $U[\sigma, \sigma_0]$ of this process is written as[9]

$$U[\sigma,\sigma_0]=\sum_{n=1}^{\infty}\int_{\sigma_0}^{\sigma} dx\,dx'\,dx_1\,dx_1'\cdots dx_n\,dx_n'\,A(x)\,\Delta(x-x')\,L(x'-x_1)\times$$
$$\times\Delta(x_1-x_1')\,L(x_1'-x_2)\cdots\times L(x_{n-1}-x_n)\,\Delta(x_n-x_n')\,B(x_n') \qquad (3.13)$$

where

$$A(x)=g_1\phi^{*\prime}(x)\psi(x) \qquad L(x)=-(g_2/2)^2 D_F(x)\,D_F'(x)$$
$$B(x)=g_2\,a(x)\,a'(x) \qquad \tfrac{1}{2}D_F(x-x')\equiv<P(a(x),a(x'))>_0 \qquad (3.14)$$
$$\Delta(x)=\tfrac{1}{2}\Delta_F(x) \qquad \tfrac{1}{2}D_F'(x-x')\equiv<P(a'(x),a'(x'))>_0$$

or in momentum space, it turns out to be

$$U[\sigma,\sigma_0]\sum_{n=0}^{\infty}\int dp\,dp_1\,dp_2\cdots dp_n\,A_{\sigma_0}^{\sigma}(p)\,\Delta(p)\,L_{\sigma_0}^{\sigma}(p,p_1)\,\Delta(p_1)\cdots\times$$
$$\times\cdots L_{\sigma_0}^{\sigma}(p_{n-1},p_n)\,\Delta(p_n)\,B_{\sigma_0}^{\sigma}(p_n) \qquad (3.15)$$

$$A_{\sigma_0}^{\sigma}=\frac{1}{(2\pi)^2}\int_{\sigma_0}^{\sigma}A(x)\,e^{ipx}dx, \qquad L_{\sigma_0}^{\sigma}(p,q)=\frac{1}{(2\pi)^4}\int_{\sigma_0}^{\sigma}L(x-y)e^{-ipx+iqy}dx\,dy \qquad (3.16)$$

$$B_{\sigma_0}^{\sigma}=\frac{1}{(2\pi)^2}\int_{\sigma_0}^{\sigma}B(x)\,e^{-ipx}dx, \qquad \Delta(p)=\frac{1}{i(p^2+m^2-i\epsilon)}$$

As the contribution from each one of the loops $L_{\sigma_0}^{\sigma}(p,q)$ can be written as

$$L_{\sigma_0}^{\sigma}(p,q)=\frac{1}{(2\pi)^4}\int_{\sigma_0}^{\sigma}e^{-i(p-q)x}dx\int_0^{(\sigma-\sigma_0)}L(y)\,e^{-iqy}dy\equiv\delta_{\sigma_0}^{\sigma}(p-q)\,L^{(\sigma-\sigma_0)}(q) \qquad (3.17)$$

we have

$$U[\sigma,\sigma_0]=\sum_{n=0}^{\infty}\int dp\,dp_1\cdots dp_n\,\delta_{\sigma_0}^{\sigma}(p-p_1)\cdots\delta_{\sigma_0}^{\sigma}(p_{n-1}-p_n)\,A_{\sigma_0}^{\sigma}(p)\,\Delta(p)\times$$
$$\times L^{(\sigma-\sigma_0)}(p_1)\,\Delta(p_1)\cdots L^{(\sigma-\sigma_0)}(p_n)\,\Delta(p_n)\,B_{\sigma_0}^{\sigma}(p_n) \qquad (3.18)$$

where

$$\delta_{\sigma_0}^{\sigma}(p-q)=\frac{1}{(2\pi)^4}\int_{\sigma_0}^{\sigma}dx\,e^{-i(p-q)x}=\delta(\boldsymbol{p}-\boldsymbol{q})\,\frac{1}{2\pi}\int_{t_0}^{t}e^{i(p_0-q_0)t'}dt' \qquad (3.19)$$

reduces to an ordinary $\delta$-functions when the time distance $t-t_0=T$ is large enough. As we are interested in the effect of the radiation damping, it is

9) D. Ito, H. Tanaka and M. Yamazaki, Prog. Theor. Phys. 7 (1952), 128 (L).

of no use to consider the behavior of the transformation function $U[\sigma, \sigma_0]$ in such a region where the temporal distance $T$ is comparable with the life time $\frac{2}{\gamma}$. Consequently, we consider the case where $mc^2 \gg \frac{\hbar\gamma}{2} \gg \hbar/T$ holds. Then all $\delta^{\sigma}_{\sigma_0}(p)$ may be replaced by ordinary $\delta(p)$, $L^{(\sigma-\sigma_0)}(p)$ by $-\Gamma(p)$, and $\frac{1}{\Delta(p)} + L^{(\sigma-\sigma_0)}(p)$ by $i\left[p^2+(m^2+\delta m^2(p))+ip_0\frac{\gamma(p)}{2}\right]$, so $U[\sigma, \sigma_0]$ becomes

$$U[\sigma, \sigma_0] = \int_{\sigma_0}^{\sigma} dx\, dx'\, A(x)\, \tfrac{1}{2}\, \Delta_D(x-x')\, B(x') \tag{3.20}$$

where

$$\Delta_D(x) = \frac{-2i}{(2\pi)^4}\int \frac{e^{ipx}}{p^2+(m^2+\delta m^2(p))-ip_0\,\gamma(p)/2-i\epsilon}\,(dp) \tag{3.21}$$
$$= e^{-\frac{1}{2}\gamma(\partial)t}\Delta'_F(x)$$

Performing the space integral, we have

$$U[\sigma, \sigma_0] \cong (2\pi)^3 A(0)\, B(0)\int \delta(P-K-K')dP\int_{-\infty}^{+\infty}\frac{dp_0/2\pi}{\epsilon_p^2-p_0^2+ip_0\,\gamma(p)/2}\times$$
$$\times\left(\frac{1-e^{i(\epsilon_k+\epsilon_{k'}-P_0)t}}{\epsilon_k+\epsilon'_k-p_0}+\frac{1-e^{-i(\epsilon_k+\epsilon_{k'}-P_0)(T-t)}}{\epsilon_k+\epsilon_{k'}-p_0}\right) \tag{3.22}$$

When the mass $m$ of the intermediate particle is large, the second term is small enough to be neglected in comparison with the first term in this sharp resonance approximation. Then,

$$W(t) \cong \frac{(g_1 g_2)^2}{(2\pi)^5}\int \frac{dP\,dK}{16\,E_p(E_p-e_p)\,\epsilon_k\epsilon'_{p-k}}\,\frac{1}{e_p^2}$$
$$\int_{-\infty}^{\infty} dP_0\,\frac{(1-e^{-\frac{\gamma t}{2}})^2+4e^{-\frac{\gamma t}{2}}\sin^2(p_0-e_p)\frac{t}{2}}{(p_0-e_p)^2+(\gamma(p)/2)^2}\,\delta(p_0-\epsilon_k-\epsilon'_{p-k}) \tag{3.23}$$

Using the formula

$$\int_{-\infty}^{+\infty}\frac{(1\,;\sin^2\frac{\omega t}{2})}{\omega^2+(\gamma/2)^2}\,d\omega = \frac{2\pi}{\gamma}\left(1\,;\,(1-e^{-\frac{\gamma t}{2}})\right) \tag{3.24}$$

we have

$$W(t) = 2\pi g_1^2\int\frac{(dP)/(2\pi)^3}{\delta E_p(E_p-e_p)\,e_p}\,(1-e^{-\gamma(\partial)t}) = \int dP\,\Gamma(P)(1-e^{-\gamma(\partial)t}) \tag{3.25}$$

This asymptotic time dependence of the transition probability has just the same form as that of (3.1). It is observed here that the effect of the detailed properties of the second decay is fading away exponentially from the expression of the transition probability, and after a long time the expression tends to the result previously calculated from the S-matrix. Thus, we have obtained the divergence-free and physically acceptable result.

(4) *several remarks*

In the same way as above, the incident line in Fig. 7 must be corrected as illustrated in Fig. 8. Then, if the rate of the first decay is greater than that of the second, the detailed nature of the first decay will fade away from the expression of the transition probability as if the history of the creation of intermediate state were completely forgotten. Such situation are frequently met in the theory of the nucler reactions, such as the compound nucleus etc., or in the case of the Hohlraumstrahlung and in the Fermi's theory[10] of multiple production of mesons.

In the nuclear processes, $\pi^0$-meson can decay into two photons through the virtual as well as the real state. Roughly speaking with our method, the decay constant $\frac{\hbar\gamma}{2}$ is so small compared with the meson mass $mc^2$ that the decay process through virtual states will be very rare.

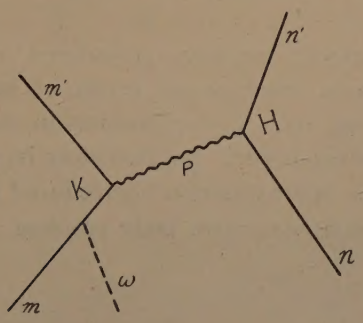


Fig. 9. ——— nucleon line, ~~~~~ meson line, ------ photon line.
$m$, $m'$, $n$ and $n'$ are nucleon states. $K$ and $H$ are their interactions.

Next, we consider the photo-nuclear effect. It is often said that in these processes the mesons emitted and then re-absorbed in the nucleus play the important roles.[11,12] At high energy, the cross-section depends mostly on the character of meson-production only and the detailed nature of meson-absorption is not important. This is just the effect of damping by absorption, and will be treated well according to our method. We take here only the simplest case. (See Fig. 9) The transformation matrix $M$ becomes

$$M=\int K(x)\,\Delta_D(x-x')\,H(x')=\int d\vec{r}\,dt\,K(\vec{r}t)\,e^{i(E_n-E'_{n'})t}\int d\vec{\xi}\,H(\vec{r}+\vec{\xi},0)\times$$

$$\times\int_{-\infty}^{\infty}d\tau\,\Delta_D(\vec{\xi},\tau)\,e^{-i(E_n-E'_{n'})\tau}\equiv\int d\vec{r}\,d\vec{r}'\,\bar{K}(\vec{r})\,G(\vec{r}-\vec{r}')\,\bar{H}(\vec{r}') \qquad (3.26)$$

10) E. Fermi, Prog. Theor. Phys. 5 (1950), 570.
11) S. Kikuchi, Phys. Rev. 85 (1951) 1062 and ibid 86 (1952) 41.
12) R. Wilson, Phys. Rev. 86 (1952), 125.

where

$$G(\vec{r}) \equiv \int^{\infty} \Delta_D(\vec{r}, t)\, e^{-i\Delta E t}\, dt = \frac{-2i}{(2\pi)^3} \int dP \frac{e^{i\vec{p}\cdot\vec{r}}}{P^2+\mu^2-(\Delta E)^2-i\Gamma(\Delta E)}$$

$$= \frac{i}{4\pi} \frac{e^{iPr}}{r} \tag{3.27}$$

$$P \equiv \sqrt{(\Delta E)^2-\mu^2+i\Gamma(\Delta E)}, \qquad \Gamma(\Delta E) = \Delta E \cdot \gamma(\Delta E)$$

Assuming the absorbing-source density is uniform in the nuclear radius $R$, and after some approximate calculation we obtain the following form†), ††)

$$|M|^2 \sim \frac{1}{4\pi} |\bar{K}\cdot\bar{H}|^2 \lambda(\Delta E)\left(1-e^{-\frac{R}{\lambda(\Delta E)}}\right) \tag{3.28}$$

where $\frac{1}{\lambda(\Delta E)} \equiv \frac{\gamma(\Delta E)}{v(\Delta E)}$, $v(\Delta E) \equiv \frac{\partial(\Delta E)}{\partial \bar{P}}$ $\bar{P}(\Delta E) \equiv \sqrt{(\Delta E)^2-\mu^2}$

Therefore, a picture of the free path of meson is asymptotically contained in this problem.

In our above treatment we have considered only a correction of the internal line by the lowest order proper graph of self-energy. According to Dyson's integral equation, our method consists in the replacement of $\Sigma^*$ by its first term $\Sigma_2^*$ in the expansion. So, this may be regarded as one-particle analogue of the "ladder approximation" introduced by Bethe and Salpeter[13] in their theory of the relativistic two body problem.

---

†) We expand $P \equiv \sqrt{(\Delta E)^2-\mu^2+i\Gamma(\Delta E)}$ in powers of $\Gamma(\Delta E)$

††) $v(\Delta E) \equiv \frac{\partial(\Delta E)}{\partial \bar{P}}$ has some approximate meaning of (group) velocity of mesons.

13) E. E. Salpeter and H. A. Bethe, Phys. Rev. 84 (1951), 1232.

昭和二十九年 四 月 二十 日印刷
昭和二十九年 四 月二十五日発行

横浜市南区大岡町
編輯兼発行者 横浜国立大学

東京都港区芝浦一ノ一
印刷者 富田元

東京都港区芝浦一ノ一
印刷所 ヘラルド社

## CONTENTS